Multiphonon excitations in boson quantum films

B. E. Clements*
Institute Laue Langevin, 38042 Grenoble Cedex, France
and Department of Physics, Texas A&M University, College Station, Texas 77843

E. Krotscheck
Institut für Theoretische Physik, Johannes Kepler Universität, A-4040 Linz, Austria
and Department of Physics, Texas A&M University, College Station, Texas 77843

C. J. Tymczak†
Department of Physics, Texas A&M University, College Station, Texas 77843
(Received 5 September 1995; revised manuscript received 22 November 1995)

Dynamical excitations in thin liquid films of ^{4}He adsorbed to a substrate are investigated by using a microscopic theory of excitations that includes multiple-phonon scattering. We study the dispersion relation, excitation mechanisms, transition densities, and particle currents as a function of surface coverage. A primary new result is that we have included three-phonon scattering processes in the calculation of the dynamic structure function and the one-body current densities. With the exception that our ground state is determined by our variational theory, rather than taken from experiment, our work on the dynamic structure function is the generalization of that of Jackson [Phys. Rev. A **4**, 2386 (1971)] to inhomogeneous systems (films). Using sum rules for the dynamic structure function as a guide, we suggest a simple scaling argument for improving the agreement between our dynamic structure function and the experimental one. The addition of three-phonon contributions bring about the following changes. First, the energy of most modes is lowered by a non-negligible amount for finite momentum excitations. Second, the film's surface mode is the exception; it is only slightly affected. Third, for monolayer films there is large scattering at high energies at intermediate values of momenta. This scattering can be traced back to an anomalously large contribution to the two-particle density of states. Fourth, all modes with energy above a critical energy decay, and the associated peaks of the dynamic structure function are broadened. Fifth, the maxonlike character is enhanced in the bulklike modes.

I. INTRODUCTION

The dynamic structure function, $S(k,\omega)$, provides useful information about the strength, lifetime, and dispersion of the dynamical excitations of a quantum fluid. Inelastic neutron scattering experiments performed at the Institute Laue-Langevin's (ILL) neutron scattering facility, on atomically thin liquid ^{4}He films, have measured a dynamic structure function that is rich in structure and complexity. To gain a full understanding of the experimental $S(k,\omega)$ for this system requires precise theoretical guidance. This is the motivation for the present work.

In contrast to the bulk system, the interpretation of the experimental $S(k,\omega)$ in terms of fundamental excitations is hampered by both experimental complications and the richness of the types of excitations. Expounding on the first point, the intensity of experimental scattering peaks scales approximately with the amount of ^{4}He present; in thin films a typical scattering peak in $S(k,\omega)$ may be 3 or 4 orders of magnitude less than scattering peaks measured in the bulk system. Even with the enormous abilities of the ILL's neutron source and detectors, the thin film's scattering peaks, corresponding to excitations of physical interest, are never considerably larger than peaks that can be attributed to statistical fluctuations (noise). Furthermore, aside from well-defined low energy Bragg peaks coming from scattering off of the underlying solid substrate, scattering intensity arising from multiple scattering off the substrate-liquid system occurs. In very thick films, this does not introduce any real complication; multiple scattering between the liquid roton excitation and the Bragg peak produces a dispersionless ''flat'' mode with energy of roughly the roton gap energy and an intensity which is orders of magnitude less than the bulk modes. In thin films it is not clear *a priori* that the multiple scattering modes should be as easily discernable from the liquid modes. In part, this complication arises, as we discuss momentarily, because the single phonon-maxon-roton in the bulk limit is replaced by a set of modes in thin liquid films. Consequently it is possible to have multiple scattering occurring from a set of modes in the thin film system.

Pertaining to the second point, it is known from previous studies that, already at the most basic level of the Feynman theory, the *single* phonon-maxon-roton dispersion curve in the bulk is replaced by a *set* of modes in the films. These modes propagate at frequencies in close proximity to one another (indeed mode crossings are not uncommon) and can be categorized as being surface modes, layer phonons, and (for thicker films) bulklike modes. Sorting out these various modes in the experiment (if they exist) is not a trivial task — again the need for a quantitative first principles theory becomes apparent.

This paper follows a series of others[1,2] (hereafter referred to as papers I and II), which were devoted to the microscopic

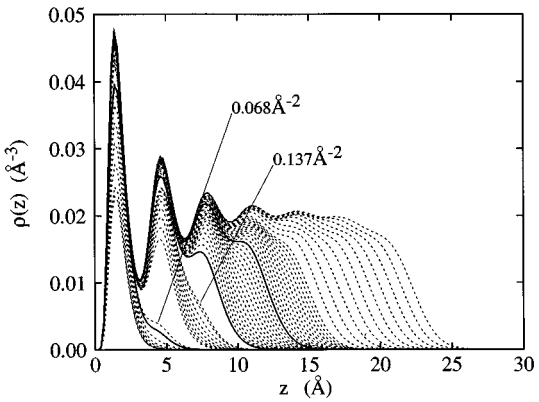

FIG. 1. A family of density profiles of ^{4}He films on a graphite-solid helium substrate are shown. The coverages are $n=0.033$, 0.035, 0.040, ..., 0.065, 0.068Å^{-2} for monolayers, $n=0.100$, 0.105, ..., 0.135, 0.137 Å^{-2} for double layers, and $n=0.165$, 0.170, ..., 0.300, 0.315, ..., 0.435, 0.450Å^{-2} for thicker films. The coverages considered in this paper $n=0.065$, 0.165, and $n=0.240$Å^{-2} are highlighted as heavy solid lines.

study of the structure and the dynamics of monolayer and multilayer helium films. An accompanying paper[3] will discuss the neutron scattering experiments, the data analysis, and the interpretation of the data. The system under consideration is comprised of a liquid helium film adsorbed to a solid ^{4}He bilayer which itself is physisorbed to a graphite substrate. The ground-state structure of this system and our theoretical tools, specifically the optimized hypernetted-chain (HNC-EL) theory, have been discussed in detail in paper I (see also Ref. 4). The films are highly layered in the sense that their density profiles show a number of distinct oscillations persisting considerable distance from the substrate. We represent the inert substrate and the two layers of solid helium by an external substrate potential $U_{\rm sub}(z)$, which is taken to depend only on the coordinate z. As a consequence, the liquid is translationally invariant in the x-y plane and exhibits a layered density profile in the z direction. A peculiarity of the system is that stable, translationally invariant configurations *cannot* be obtained for all surface coverages; we refer the reader to paper I for a discussion of this.

For further reference, we show in Fig. 1 a set of density profiles for helium films on the above-mentioned substrates. These profiles are characterized by the surface coverage

$$n=\int dz\rho_1(z). \tag{1.1}$$

The void regions between $n=0.068$ Å^{-2} and $n=0.1$ Å^{-2} as well as between $n=0.137$ Å^{-2} and $n=0.165$ Å^{-2} are the areas where no translationally invariant configurations of the system exist. These areas depend to a large extent on the *range* of the substrate potential; long-range potentials typically tend to show fewer regimes of instability, cf. Ref. 4. The calculations of the present paper concentrate on a few typical examples: a monolayer film with $n=0.065$ Å^{-2}, and a triple and quadruple layer film with $n=0.165$ Å^{-2} and $n=0.240$Å^{-2}, respectively. These examples are highlighted in Fig. 1.

In paper II, we have examined the nature of the film's low-lying excited states. The theory mostly used there provided an intuitive and qualitatively reasonable picture of the low-lying excitations of such systems, but it had a number of quantitative deficiencies. In an attempt to provide more reliable estimates for the dispersion curves of higher-lying excitations, and the intensities and linewidths of the scattering peaks in $S(k,\omega)$, the present work has several improvements over these earlier calculations; in particular we include multiphonon contributions in the current densities and the $S(k,\omega)$. Our theory for determining multiphonon contributions to the $S(k,\omega)$ will be considered in detail in the next section; here we make a few introductory comments. At the heart of the approach is the fundamental theory first proposed by Saarela *et al.* for bulk quantum fluids,[5–7] and then developed for the study of excitations in quantum film structures.[2]

If a small time-dependent perturbation momentarily drives the film out of its ground state, a logical extension of the usual Jastrow-Feenberg variational wave function to excited states is

$$|\Psi(t)\rangle=\frac{e^{-iE_0t/\hbar}e^{(1/2)\delta U(t)}|\Psi_0\rangle}{[\langle\Psi_0|e^{\delta U(t)}|\Psi_0\rangle]^{1/2}}\equiv e^{-iE_0t/\hbar}|\Psi_0(t)\rangle, \tag{1.2}$$

where $|\Psi_0\rangle$ is the ground-state wave function, E_0 is its energy, and

$$\delta U=\sum_i \delta u_1(\mathbf{r}_i;t)+\sum_{i<j}\delta u_2(\mathbf{r}_i,\mathbf{r}_j;t)+\cdots, \tag{1.3}$$

is the complex *excitation operator*.

The time-dependent correlations, $\delta u_n(\mathbf{r}_1,\ldots,\mathbf{r}_n;t)$, are determined by an action principle:[8,9]

$$\delta\mathscr{S}=\delta\int dt\left\langle\Psi(t)\left|H-i\hbar\frac{\partial}{\partial t}\right|\Psi(t)\right\rangle=0. \tag{1.4}$$

where the variations are taken treating the $\delta u_n(\mathbf{r}_1,\ldots,\mathbf{r}_n;t)$ as independent functions.[2,5–7] In Eq. (1.4), H is the Hamiltonian for the perturbed system

$$H=\sum_{i=1}^{N}\left\{-\frac{\hbar^2}{2m}\nabla_i^2+U_{\rm sub}(\mathbf{r}_i)+U_{\rm ext}(\mathbf{r}_i;t)\right\}$$
$$+\sum_{1\le i<j\le N}v(|\mathbf{r}_i-\mathbf{r}_j|)=H_0+\delta H(t), \tag{1.5}$$

where $U_{\rm sub}(\mathbf{r})$ is an external static ''substrate'' potential, and $v(|\mathbf{r}_i-\mathbf{r}_j|)$ is the interaction between individual particles, which we take to be the Aziz potential.[10] The time-dependent part

$$\delta H(t)=\sum_i U_{\rm ext}(\mathbf{r}_i;t) \tag{1.6}$$

describes an external scalar perturbation which we assume is sufficiently small to permit a linearization of the equations of motion in terms of the $\delta u_n(\mathbf{r}_1,\ldots,\mathbf{r}_n;t)$. By keeping terms with leading order in the dynamical correlations, the resulting Euler equations can be cast in the form of coupled *equa-*

tions of motion (EOM). The conjugate variable to the time is the excitation energy, $\hbar\omega$. In general it is complex; the real part is the excitation's dispersion and the imaginary part gives its inverse lifetime.

The truncation of the excitation operator (1.3) defines the level of approximation in which we treat the excitations. The simplest approximation, which ignores all fluctuating correlation functions except $\delta u_1(\mathbf{r};t)$ is referred to, hereafter, as the *Feynman approximation.* In this case the resulting ω is purely real. This approximation leads, in the bulk limit, to the well-known Feynman dispersion relation $\hbar\omega(k)=\hbar^2k^2/2mS(k)$. It is a reasonable approximation as long as the wavelength of the excitation is large compared to the average particle spacing; in particular, it is exact in the long-wavelength limit. Subsequent work of Feynman and Cohen[11] and Feenberg and co-workers[12–14] showed that while the theory is qualitatively correct, higher order scattering processes (involving multiple Fourier components) are essential for a full understanding of the excitation spectrum. In the short-wavelength regime (above 1.0 Å^{-1}) the Feynman approximation significantly overestimates the excitation energy, and keeping $\delta u_2(\mathbf{r}_i,\mathbf{r}_j;t)$ leads to a significant lowering of the excitation energy.[5–7]

In the film problem a full evaluation of the EOM for fluctuating pair correlations is numerically very time consuming and approximations are necessary. The approximation that we will use is tantamount to keeping ''three-phonon scattering processes.'' (Parenthetically, this nomenclature is conventional but should not to be taken literally since the coupling matrix element may be between layer phonons and surface modes, for example.) In bulk ^{4}He, the Feynman approximation and theories that include three-phonon contributions differ in two significant ways. First, in the latter theory the magnitude of the excitation energy is reduced from the Feynman value, especially for wavelengths corresponding to the bulk maxon and roton. This is desirable since the Feynman approximation overestimates the roton minimum in the bulk by a factor of 2. One should not expect *a priori* that the different modes in the Bose film will be reduced by the same amount; the physical character of the various modes differs considerably and this will play an important role in determining the amount that a particular mode is renormalized by three-phonon processes. Second, in the latter theory, above a given critical energy, $\hbar\omega_c$ the modes are complex, i.e., they will have a linewidth which reflects the inverse lifetime of the mode.

Our paper is organized as follows: In the next section, we will outline a general theory of excited states which is based on the concept of fluctuating correlation functions, alluded to above. We will formulate the equations of motion for time-dependent one-body and two-body correlations. Input to the theory are one-body and two-body densities obtained from the ground-state calculations. In the limit that only single-particle functions are allowed to be time dependent, the theory reduces to the generalized Feynman theory of collective excitations. This section will essentially display only the first and the last step of the analytical manipulations. In an attempt to improve the readability of the paper we have saved the majority of the technical points for a set of appendices. These present the details of the derivation of the equations of motion (Appendix A), the approximations that we use (Appendix B), a proof of sum rules for the generalized theory (Appendix C), and the calculation of particle currents (Appendix D).

Section III is devoted to the applications of our theory. We first discuss the essence of our working formulas and possibilities to introduce phenomenological input to the theory. We then apply the theory to the bulk two- and three-dimensional liquid and calculate both the phonon-roton spectrum and the static response function. Having convinced ourselves that the theory provides quite satisfactory agreement with *known* data, we then proceed to apply our theory to a study of the excitations of a representative sample of liquid monolayer and multilayer films. In these more complicated geometries, we will find a multitude of different excitations corresponding to surface phonons (''ripplons'' and/or ''third sound'') and volume excitations (''bulk phonons'') which may be confined to individual liquids layers (''layer phonons''). To achieve an appreciation of full scope of possible mechanisms, we study the particle currents. Finally, Sec. IV contains a brief summary of our results.

II. THEORY OF MULTIPHONON EXCITATIONS

This section contains the basic ideas of the method of fluctuating multiparticle correlations and the working formulas of our theory. Details on the somewhat lengthy algebraic manipulations are presented in Appendices A and B. We start with the action principle (1.4), and assume an excitation operator that includes time-dependent one-body and two-body components,[5] i.e., we assume

$$\delta U(t)=\sum_i \delta u_1(\mathbf{r}_i;t)+\sum_{i<j}\delta u_2(\mathbf{r}_i,\mathbf{r}_j;t). \tag{2.1}$$

Taking into account the explicit time dependence of the wave function spelled out in Eq. (1.2), the action principle (1.4) assumes the form

$$\mathcal{S}=\int dt\,\mathcal{L}(t)=\int dt\left\langle \Psi_0(t)\left|H-E_0-i\hbar\frac{\partial}{\partial t}\right|\Psi_0(t)\right\rangle. \tag{2.2}$$

If the time-dependent part of the correlations is small, we can expand the Lagrangian to second order in $\delta U(t)$

$$\begin{aligned}\mathcal{L}(t)=&\frac{1}{8}\langle\Psi_0|[\delta U^*,[T,\delta U]]|\Psi_0\rangle\\&-\frac{i\hbar}{8}\left[\left\langle\Psi_0\left|\delta\dot{U}[\delta U^*-\langle\Psi_0|\delta U^*|\Psi_0\rangle]\right|\Psi_0\right\rangle\right.\\&\left.-\text{c.c.}\right]+\left\langle\Psi_0(t)\left|\sum_i U_{\text{ext}}(\mathbf{r}_i;t)\right|\Psi_0(t)\right\rangle.\end{aligned} \tag{2.3}$$

The original Feynman theory of collective excitations[15] is obtained by restricting the excitation operator (2.1) to the one-body component $\delta u_1(\mathbf{r}_i;t)$. Since the ''Feynman-phonon'' states also form a convenient basis for the formulation of the generalized theory, we shall review this ap-

proach briefly. Omitting $\delta u_2(\mathbf{r}_i,\mathbf{r}_j)$ in $\delta U(t)$, the Lagrangian (2.3) can be expressed in terms of one-body and two-body densities,

$$\mathscr{L}_1(t)=\frac{\hbar^2}{8m}\int d^3r\,\rho_1(\mathbf{r})|\nabla\delta u_1(\mathbf{r};t)|^2 - \frac{i\hbar}{8}\int d^3r\,\dot{\rho}_1(\mathbf{r};t)\,\delta u_1^*(\mathbf{r};t) + \int d^3r\,U_{\rm ext}(\mathbf{r};t)\mathrm{Re}\rho_1(\mathbf{r};t), \tag{2.4}$$

where, to first order in the time-dependent function,

$$\rho_1(\mathbf{r};t)=\rho_1(\mathbf{r})+\delta\rho_1(\mathbf{r};t),$$

$$\delta\rho_1(\mathbf{r};t)=\rho_1(\mathbf{r})\,\delta u_1(\mathbf{r}';t)+\int d^3r'[\rho_2(\mathbf{r},\mathbf{r}') - \rho_1(\mathbf{r})\rho_1(\mathbf{r}')]\delta u_1(\mathbf{r}';t). \tag{2.5}$$

Note that in Eq. (2.5) $\delta\rho_1(\mathbf{r};t)$ is complex; the physical density fluctuation is the real part of this function. In these equations, the n-body densities are defined by

$$\rho_n(\mathbf{r}_1,\cdots,\mathbf{r}_n)=\frac{N!}{(N-n)!}\,\frac{\int d^3r_{n+1}\cdots d^3r_N\Psi_0^2(\mathbf{r}_1,\ldots,\mathbf{r}_N)}{\int d^3r_1\ldots d^3r_N\Psi_0^2(\mathbf{r}_1,\ldots,\mathbf{r}_N)}, \tag{2.6}$$

and the corresponding distribution functions by

$$g_n(\mathbf{r}_1,\ldots,\mathbf{r}_n)=\frac{\rho_n(\mathbf{r}_1,\ldots,\mathbf{r}_n)}{\rho_1(\mathbf{r}_1)\cdots\rho_1(\mathbf{r}_n)}. \tag{2.7}$$

The manipulations needed to derive the fluctuating part of the density in terms of the time-dependent external field are a subset of those carried out in Appendix A; they may also be found in Ref. 16. It is convenient to work in the space spanned by the eigenfunctions of a generalized Feynman eigenvalue problem. Assuming harmonic time dependence, $\delta u_1(\mathbf{r};t)=\delta u_1(\mathbf{r})e^{i\omega t}$, and defining

$$\psi(\mathbf{r})=\sqrt{\rho_1(\mathbf{r})}\,\delta u_1(\mathbf{r}), \tag{2.8}$$

the solution of the action principle (1.4) may be represented by the solutions $\psi^{(n)}(\mathbf{r})$ of the generalized eigenvalue problem

$$H_1\psi^{(n)}(\mathbf{r})=\hbar\omega_n\int d^3r'\,S(\mathbf{r},\mathbf{r}')\psi^{(n)}(\mathbf{r}') \tag{2.9}$$

with the coordinate space representation of the static structure function

$$S(\mathbf{r},\mathbf{r}')=\delta(\mathbf{r}-\mathbf{r}')+\frac{\rho_2(\mathbf{r},\mathbf{r}')-\rho_1(\mathbf{r})\rho_1(\mathbf{r}')}{\sqrt{\rho_1(\mathbf{r})\rho_1(\mathbf{r}')}} \tag{2.10}$$

and the kinetic energy operator

$$H_1=-\frac{\hbar^2}{2m}\,\frac{1}{\sqrt{\rho_1(\mathbf{r})}}\nabla\rho_1(\mathbf{r})\nabla\,\frac{1}{\sqrt{\rho_1(\mathbf{r})}}. \tag{2.11}$$

The bulk limit of the eigenvalue problem (2.9) is the Feynman dispersion relation $\omega(k)=\hbar k^2/2mS(k)$. A convenient normalization of the eigenstates of the generalized eigenvalue problem (2.9) is

$$(\psi^{(m)}|H_1|\psi^{(n)})=\hbar\omega_m\delta_{mn}. \tag{2.12}$$

These eigenstates are related to the Feynman excitation functions $\delta u_1(\mathbf{r})$ through Eq. (2.8). The adjoint states

$$\phi^{(m)}(\mathbf{r})\equiv\frac{1}{\hbar\omega_n}H_1\psi^{(n)}(\mathbf{r}) \tag{2.13}$$

are related to the physical density fluctuations (cf. Refs. 16 and 2)

$$\delta\rho_1(\mathbf{r})=\sqrt{\rho_1(\mathbf{r})}\,\phi^{(n)}(\mathbf{r}). \tag{2.14}$$

We note in passing that the eigenstates $\phi^{(n)}(\mathbf{r})$ and $\psi^{(n)}(\mathbf{r})$ are also the essential ingredients of the solution of the Euler equation for the pair correlations and provide a convenient basis for the representation of optimized triplet correlations.[1]

Within the Feynman approximation, which corresponds here to the random phase approximation (RPA), we construct from these states the density-density response function:

$$\chi^{\rm RPA}(\mathbf{r},\mathbf{r}',\omega)=\sqrt{\rho_1(\mathbf{r})}\sum_{st}\,\phi^{(s)}(\mathbf{r})[G_{st}^{\rm RPA}(\omega)+G_{st}^{\rm RPA}(-\omega)]\phi^{(t)}(\mathbf{r}')\sqrt{\rho_1(\mathbf{r}')}, \tag{2.15}$$

where

$$G_{st}^{\rm RPA}(\omega)=\frac{\delta_{st}}{\hbar[\omega-\omega_s+i\epsilon]} \tag{2.16}$$

is the Greens' function for a free Feynman phonon. The static form factor is calculated from the response function (2.15) by frequency integration:

$$S(\mathbf{r},\mathbf{r}')=-\frac{1}{\sqrt{\rho_1(\mathbf{r})\rho_1(\mathbf{r}')}}\int_0^\infty\frac{d(\hbar\omega)}{\pi}\mathrm{Im}\chi^{\rm RPA}(\mathbf{r},\mathbf{r}';\omega)=\sum_s\,\phi^{(s)}(\mathbf{r})\phi^{(s)}(\mathbf{r}'). \tag{2.17}$$

We note that this ''RPA'' static structure function obtained here, by frequency integration of the response function, is *identical* to the one obtained in the ground-state calculation. In the latter calculation, excitations are not involved in any explicit way.

In Appendices A and B, we derive an improved expression for the dynamic response function by including three-phonon scattering processes. We shall call the resulting response function the CBF response function, after the first derivation[14] of this form within the theory of correlated basis functions (CBF's). In terms of the Feynman states introduced above, this response function also has the form (2.15), i.e.,

$$\chi^{\mathrm{CBF}}(\mathbf{r},\mathbf{r}',\omega)=\sqrt{\rho_1(\mathbf{r})}\sum_{st}\ \phi^{(s)}(\mathbf{r})[G_{st}^{\mathrm{CBF}}(\omega)+G_{st}^{\mathrm{CBF}}(-\omega)]\phi^{(t)}(\mathbf{r}')\sqrt{\rho_1(\mathbf{r}')} \tag{2.18}$$

but where now

$$G_{st}^{\mathrm{CBF}}(\omega)=[\hbar[\omega-\omega_s+i\epsilon]\delta_{st}+\Sigma_{st}(\omega)]^{-1} \tag{2.19}$$

is the CBF Greens's function, with the self-energy correction

$$\Sigma_{st}(\omega)=\frac{1}{2}\sum_{mn}\ \frac{V_{mn}^{(s)}V_{mn}^{(t)}}{\hbar(\omega_m+\omega_n-\omega+i\epsilon)}, \tag{2.20}$$

where the $V_{mn}^{(s)}$ are three-phonon coupling matrix elements and are given in Appendix B. The *normal modes* of the system are determined by the poles of the Green's function, or the zeros of its inverse

$$E_{st}^{\mathrm{CBF}}(\omega)=\hbar[\omega-\omega_s+i\epsilon]\delta_{st}+\Sigma_{st}(\omega), \tag{2.21}$$

in other words by the nonlinear eigenvalue problem

$$\hbar\omega_s\varphi_s-\frac{1}{2}\sum_{mn}\ \frac{V_{mn}^{s}V_{mn}^{t}}{\hbar(\omega_m+\omega_n-\omega)}\varphi_t=\hbar\omega\varphi_s. \tag{2.22}$$

The time-dependent part of the density can then be expressed as a linear superposition of the Feynman density fluctuations,

$$\delta\rho_1(\mathbf{r})=\sqrt{\rho_1(\mathbf{r})}\sum_{n}\ \varphi_n\phi_n(\mathbf{r}). \tag{2.23}$$

Equation (2.22) has evidently the structure of a Brillouin-Wigner (BW) perturbation formula, we will therefore refer to the theory as correlated-basis-function Brillouin-Wigner (CBF-BW) expression.

We now argue that a major strength of the present theory is that it does not compromise the precision of quantities that were calculated with great precision in the ground-state theory. The important quantity to consider is the static structure function. In paper I, it is shown that the static structure function, and the related pair distribution function, determined from the ground-state theory, agree to great accuracy with the experimentally determined bulk quantities. The Feynman theory, by definition, does not change the static structure function. The obvious question that arises is, how much, if at all, will the ground-state static structure function differ from one produced by the frequency integration of the CBF-BW dynamic response function:

$$S^{\mathrm{CBF}}(\mathbf{r},\mathbf{r}')=-\frac{1}{\sqrt{\rho_1(\mathbf{r})\rho_1(\mathbf{r}')}}\int_0^\infty\frac{d(\hbar\omega)}{\pi}\mathrm{Im}\chi^{\mathrm{CBF}}(\mathbf{r},\mathbf{r}';\omega). \tag{2.24}$$

For the *homogeneous* system it has been proven by Jackson[17] that the static structure function obtained from the multiphonon theory is *identical* to the one obtained in the Feynman theory and, hence, in the ground-state calculation. In other words, the introduction of multiphonon processes merely causes a shift and redistribution of spectral weights in the dynamic structure function, but does not change the frequency integrals. It is plausible that the same statement should be true in the inhomogeneous geometry, however the proof of the theorem is nontrivial and will be presented in Appendix C. It would be interesting to carry out a similar analysis on the density-functional approach proposed in Ref. 18. By introducing a Gaussian current-current coupling term in the density functional, containing several adjustable parameters, these authors obtain a very good fit to the bulk static response function and the phonon-roton spectrum. The validity of the parametrization can, of course, be assessed only by comparison to results that are sufficiently well known, but were not used for the choice of the energy functional. The static structure function, the spectrum of higher-lying ''multiphonon'' excitations, and the natural broadening of these excitations due to phonon decay would be a prime candidate for such consistency tests.

III. APPLICATIONS OF THE THEORY

A. Practical considerations

Before we turn to the numerical application of our theory we would like to discuss why we feel that our approach is appropriate, and why it describes the correct physics; what the approximations are and how these approximations could be improved; and how potentially phenomenological input may be used to circumvent the most laborious and unrewarding aspects of the microscopic theory.

Formally, the method of *time-dependent* multiparticle correlations is the logical extension of the variational method for the ground state. The question arises, of course, *which* portion of the correlations must be allowed to be time dependent in order to correctly describe the physics of a specific excitation. In that respect, it is perfectly plausible that long-wavelength excitations are described well by allowing for a fluctuating one-body component only. It is equally plausible and well established that such an approximation becomes invalid when the wavelength of the excitation is comparable to the average particle separation. Letting correlations fluctuate that dominate the behavior of the system at these wavelengths appears to be natural from the variational point of view.

A simple consideration provides a rough estimate of the expected accuracy of theory: When *all three* correlation functions are allowed to bear the full symmetry breaking, the variational theory provides very satisfactory agreement with Monte Carlo simulations even for systems with very strong,

macroscopic density modulations.[19] Indeed, we find almost perfect agreement with Monte Carlo data for the strongest conceivable density modulation, namely the two-dimensional limit.[1] It is therefore expected that one should have equally good agreement for infinitesimally weak density fluctuations, in other words for the *static response function.* The neglect of fluctuating triplet correlations could, at worst, introduce an uncertainty of the order of the contribution of triplet correlations to the ground state, which is about 10%.[20] While this argument applies rigorously for the *static* response function only, we shall see below that both the static response function and the phonon roton dispersion relation are improved, with the degree of sophistication of the theory, at the same rate. We estimate therefore that the theory is capable — subject to the removal of some of the approximation discussed in Appendix B — of reproducing both the static response function and the phonon/roton dispersion relation within an accuracy no worse than 10%.

Our estimate is consistent with applications of the theory for the bulk liquid. By doing a rather complete evaluation of the EOM at the level of two-body time-dependent fluctuations, Saarela *et al.*[7] found an energy value of 9.7 K for the roton minium. In comparison, the experimental value[21] for the roton minimum in the bulk is 8.6 K. Furthermore, Saarela's calculated dispersion relation is in excellent agreement with experiment at momentum values well above $k=2$ Å^{-2}. The same is true for the static response function.[6]

In the nonuniform system, a calculation at the level of Ref. 7 is much more tedious and, before we embark on the numerically laborious route of improving the purely microscopic description, we shall explore simpler versions of the theory and, in a more phenomenological manner, the possible sources of mismatch between experiment and theory. As outlined in the Appendices, the numerical implementation of our theory corresponds to the generalization of the correlated basis functions theory used by Jackson,[14] Campbell,[12,22] and collaborators. The theory exhausts, at this level, somewhat over 50% of the difference between the Feynman approximation and the experiment for both the phonon-roton spectrum (Fig. 2) and the static response function (Fig. 3).

It appears that one can conclude two things from the comparison between Saarela's and Campbell's results: First, this approach correctly describes the phonon-roton spectrum observed experimentally. Second, it is apparently sufficient to include only two-body time dependent fluctuations —there is no need to include three-body or higher time dependent fluctuations. The dominant part of any discrepancy between theory and experiment lies in the actual numerical implementation of the theory at the level of fluctuating pair correlations.

Returning to the questions on which approximations are implied, and what the route of potential microscopic or phenomenological improvement could be, we assert that, from the structure (2.19) and (2.20) of the Green's function and the self-energy matrix Σ_{st} three approximations are evident.

(i) The approximation used here ignores four-phonon coupling effects. This is a consequence of our treatment of the equations of motion, specifically the ''uniform limit'' approximation.

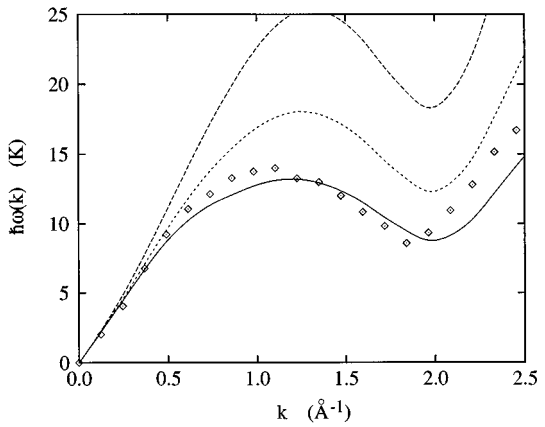

FIG. 2. The phonon-dispersion relation is shown, for bulk *three-dimensional* ^{4}He, at experimental saturation density $\rho=0.021\,85$ Å^{-3} in (a) Feynman approximation (long-dashed line) and in CBF-BW approximation (short-dashed line), (c) CBF-BW approximation with scaled spectrum (solid line), and (d) from experiments (Ref. 21) (diamonds).

(ii) The working formulas for the three-body coupling matrix elements $V^{(s)}_{mn}$, derived in Appendix B, make assumptions on the optimal triplet correlation functions,

(iii) Finally, the energy denominator of the self-energy equation (2.20) contains the Feynman phonon energies, but no further self-energy corrections. This is also a consequence of the ''uniform limit'' approximation, more specifically the treatment of the integral operator on the left-hand side of Eq. (A18) through Eq. (B9).

B. Bulk limit in three and two dimensions

The goal of the present work is not only to present a generically microscopic theory of excitations in adsorbed films, but also to help interpret the rich and complicated experimental data. We feel, therefore, free to use some infor-

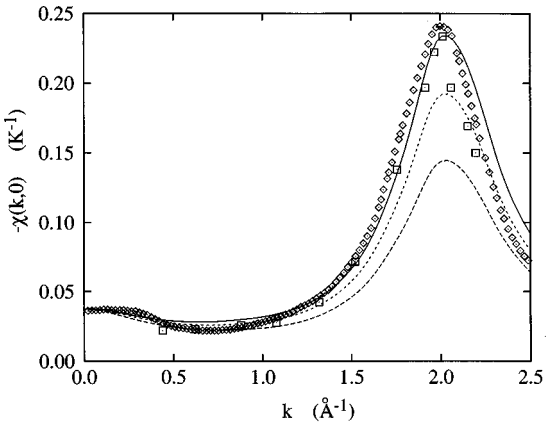

FIG. 3. The static response function $-\chi(k,0)$ is shown, for bulk *three-dimensional* ^{4}He, at experimental saturation density $\rho=0.021\,85$ Å^{-3} in (a) Feynman approximation (long-dashed line) and in CBF-BW approximation (short-dashed line), (c) CBF-BW approximation with scaled spectrum (solid line), (d) from experiments (Ref. 21) (diamonds), and (e) from Monte Carlo data (Ref. 24) (boxes).

mation on ''how an improved theory would look'' in order to modestly introduce phenomenological information.

The first point that needs clarification is to what degree our approximations effect the validity of our theoretical results, and how one can compensate for the approximations dictated by computational considerations. This is best tested in the bulk liquid, where comparisons with more complete evaluations of the EOM, experiments, and Monte Carlo data are available. From Eq. (2.22) it is obvious that two simple adjustments of the relevant quantities can be made: these are to adjust the strength of the three-body vertex, and (or) the spectrum in the energy denominator.

From our calculations on triplet correlations in the ground state in He^4 we have confidence in our calculation of the three-phonon three-body vertex. In Ref. 20 we have found that the next correction to the triplet function provides only perhaps a 10% correction to the vertex X_{ijk} [cf. Eqs. (B29) and (B31)] which itself is a small correction to the leading term $[V^t_{mn}]_0$ [Eq. (B30)] of the three-phonon vertex. Note, however, that the three-body vertex X_{ijk} in the form used here cannot be neglected since it is necessary for obtaining the correct density dependence of the roton minimum.[12]

On the other hand, it is also clear that the energy denominator in Eq. (2.22) should not contain the Feynman states, but rather the proper self-energy. To estimate the importance of this effect, one can insert the *experimental* spectrum into the energy denominators and find, indeed, a significant improvement of the spectrum. Moreover, the multiphonon continuum is correctly moved downwards in energy.

However, for the problem at hand of calculating the dynamic structure function of adsorbed films, the procedure of putting an *experimental* spectrum in the energy denominators is impractical. Instead, we have scaled the Feynman energies in the denominator to roughly agree with the experimental spectrum. For this purpose, a scaling factor of 0.6–0.65 leads to satisfactory agreement in the bulk calculation; we have used a scaling factor of 0.65 throughout all calculations. In the work below, we will refer to this as the ''scaled'' CBF-BW approximation. The results from these calculations are also shown in Figs. 2 and 3. Note that the proof of the sumrules presented in Appendix C is independent of the specific details of both the three-phonon coupling matrix elements and the spectrum in the energy denominator, hence our scaling procedure does not compromise the precision of the static structure function obtained in the ground state theory.

The agreement of the calculated spectrum with the experimental phonon-roton spectrum is promising; it could be further improved by a momentum-dependent scaling or by an independent scaling of both the interaction and the spectrum. We have refrained from such a procedure since the inclusion of more uncontrolled parameters would jeopardize the predictive power of the theory.

The validity of our procedure can, however, only be judged by looking at quantities that are well enough known to make definitive statements, but were *not* used as ''phenomenological input'' for determining the scaling of the energy denominator. A prime candidate for such data is the *density dependence* of the roton parameters. A compilation of relevant data has recently been given by Montfrooij and de Schepper (Ref. 23). Figures 4 and 5 compare these experimental data for the energy and the momentum of the roton minimum with our theoretical results. We see that the theoretical location follows closely the experimental data; our minimum being shifted consistently by 0.05 $Å^{-1}$ towards higher momenta, and the energy is accurate to within 0.5 K. The agreement is certainly satisfactory given our admittedly crude way to account for self-energy corrections.

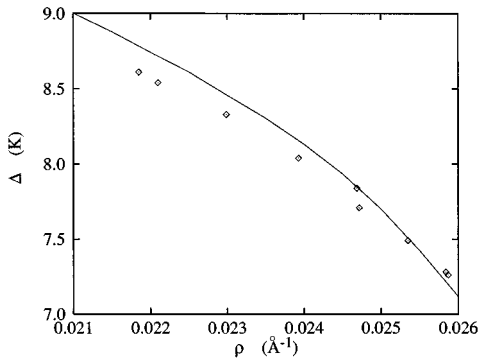

FIG. 4. The roton energy Δ is shown as a function of density. The solid line shows our calculated scaled CBF-BW results and the diamonds represent experimental data of Refs. 33–35.

Our results for the *static* response function at saturation density (Fig. 3) are particularly satisfactory. Note that *no* additional adjustments needed to be made. Figure 3 shows a comparison with both experimental data[21] and diffusion Monte Carlo simulations.[24] Apparently, our results of the scaled theory are, for momentum values *below* the maximum of the static response function, almost identical to Monte Carlo data; they deviate for wave numbers *above* that of the maximum from experiments by about the same amount as the Monte Carlo data, albeit in the opposite direction. It appears therefore that a density-density response function of the type (2.18) with the self-energy (2.20) can quite accurately describe *both static and dynamic* properties of a quantum liquid in the relevant density regime. Unfortunately, there are, to our knowledge, no experimental data for the static response function at higher densities; we have therefore resorted to comparison with Monte Carlo data by Moroni *et al.*[24] This comparison is shown in Fig. 6. At high

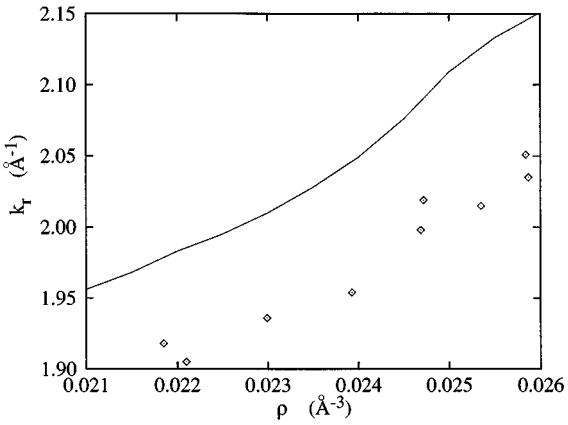

FIG. 5. Same as Fig. 4 for the wave number of the roton minimum.

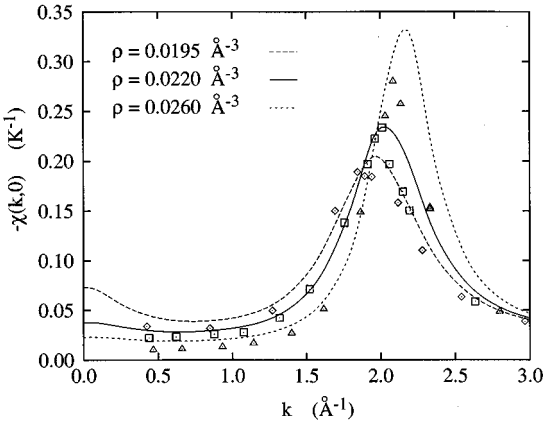

FIG. 6. The static response function $-\chi(k,0)$ is compared, for bulk *three-dimensional* ^{4}He, with Monte Carlo results of Moroni *et al.* (Ref. 24) for densities of $\rho=0.019\,64$ Å^{-3} (diamonds), $\rho=0.021\,86$ Å^{-3} (boxes), and $\rho=0.026\,22$ Å^{-3} (triangles), and our calculations for $\rho=0.0195$ Å^{-3} (long-dashed line), $\rho=0.0220$ Å^{-3} (solid line), and $\rho=0.0260$ Å^{-3} (short-dashed line).

densities, the maximum of our static response function appears to be somewhat too high compared to the Monte Carlo data. This is of no further consequence for the validity of our results since we are here concerned mainly with the *dynamic* response at densities at or below saturation densities. For the sound propagation in the highly compressed atomic monolayers close to the substrate, data on the phonon-roton spectrum in two dimensions are more relevant.

Further nontrivial predictions of our theory and in particular the treatment of self-energy corrections are the phonon-roton dispersion relation and the static structure function in two dimensions. Results are shown, for three densities below, at, and above saturation, in Figs. 7 and 8. It would be extremely interesting to verify our estimate that the unrenormalized CBF theory underestimates the importance of multiphonon corrections by about the same amount as in three

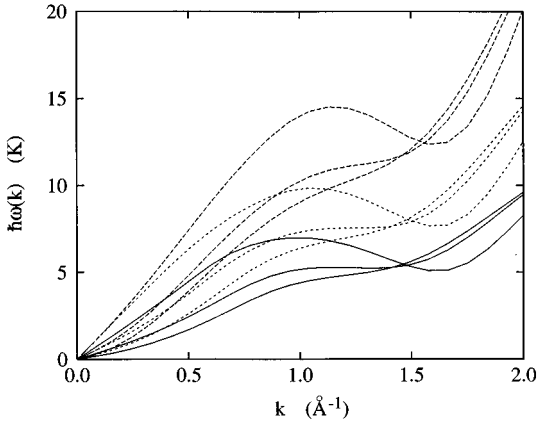

FIG. 7. The phonon-roton spectrum in *two-dimensional* ^{4}He, (a) Feynman approximation (long-dashed line), (b) CBF-BW approximation (short-dashed line), and (c) CBF-BW approximation with scaled spectrum (solid lines). Densities are $n=0.035$ Å^{-2}, $n=0.041$ Å^{-2}, and $n=0.053$ Å^{-2}, the upper curves with the lower roton minimum corresponding to the higher density.

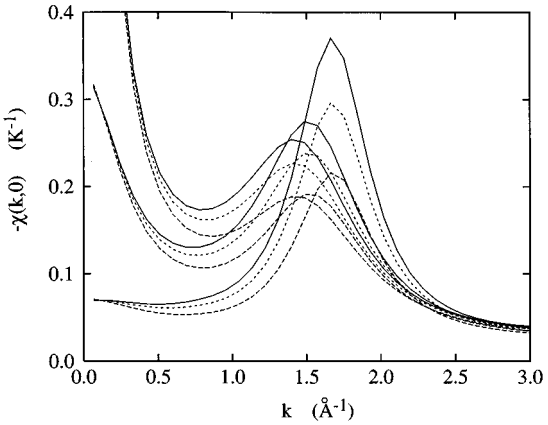

FIG. 8. Same as Fig. 7 for the static response function $-\chi(k,0)$. The functions with the higher peaks correspond to the higher densities.

dimensions, by either more complete solutions of the equations of motion[7] or by Monte Carlo calculations for the phonon-roton spectrum[25] or the static response function.[24] For our purposes, the examination of the two-dimensional limit is by-in-large a consistency test: We have seen in II that low-coverage atomic monolayers behave essentially like two-dimensional systems up to a crossover point at which the population of a second layer becomes energetically favorable over the compression of the first layer. A precursor to this transition is that a visible ripplon mode appears. On the substrate under consideration here, this happens at a crossover coverage of approximately $n\approx0.055$ Å^{-2}, the actual three-dimensional nature of the film, which is our main concern, becomes visible only above such coverages.

An extensive discussion of the dynamic structure function for the bulk liquid can be found in Ref. 14. Our calculation, has, apart from having more accurate input, not much to add to Jackson's analysis for the bulk liquid.

C. Monolayer films

1. Dynamic structure function

Let us now turn to our numerical results on excitations in adsorbed ^{4}He films. We have numerically calculated the full dynamic response function for several film thicknesses from one ($n=0.065$ Å^{-2}) to four layers ($n=0.240$ Å^{-2}). To keep the computational effort reasonable, one must limit, in Eq. (2.22), the sum over the intermediate states. We have chosen this cutoff, dependent on the momentum transfer, several degrees above the highest energy in $S(k,\omega)$ that we have considered; tests were carried out to verify the convergence. For the monolayer film this is not critical since most of the spectral weight appears in the lowest Feynman excitation. As the number of layers increase, however, the number of Feynman states needed in the summations over the intermediate states in the self-energy (2.20) increases rapidly, and the computation becomes very time consuming.

Following the strategy of paper II, we use the *transition densities* and *particle currents* to determine the nature of the modes that we observe in the dynamic structure function. We surpass that work by now including the multiphonon scattering processes, as described above. By comparing quantitative

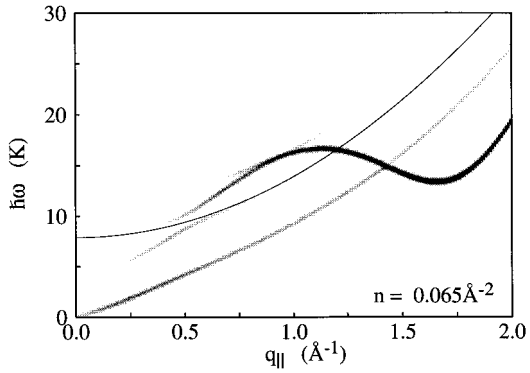

FIG. 9. The dynamic structure function in the Feynman approximation for $n=0.065$ Å^{-2} film. The solid line is the continuum boundary $\hbar\omega_{\rm cb}=-\mu+\hbar^2 q_\parallel^2/2m$. The level of grayscale indicates the strength of $S(q_\parallel,\omega)$.

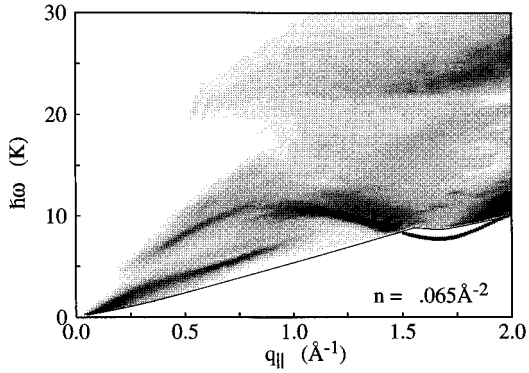

FIG. 10. The dynamic structure function in the scaled CBF approximation for $n=0.065$ Å^{-2} film. The solid line is $\hbar\omega_c$ described in the text.

differences in the Feynman and CBF-BW theories we can assess the importance of the coupling of the various modes. The appearance of scattering intensity in the CBF-BW $S(q_\parallel,\omega)$ has either a Feynman counterpart (a Feynman mode), but perhaps renormalized in energy and strength, or arises from a hybridization of Feynman states. In that case there will be no counterpart in the Feynman theory. In going from the Feynman to the CBF-BW theories, the amount of renormalization that a mode will experience depends strongly on the strength of the mode coupling [through the three-phonon vertices in Eq. (2.22)] and the energetics of the corresponding Feynman modes (the corresponding energy denominator). Such coupling of modes can be either self- or mixed-mode coupling. Self-mode coupling refers to coupling of modes with the same (Feynman) dispersion branch, for example, ripplon-ripplon coupling. The term, self-mode, cannot be taken too literally since, even in the absence of mode crossings, the nature of an excitation can change dramatically at different momenta along the same dispersion branch.[2] Similarly, mixed mode refers to the coupling between two modes having different dispersion branches. As a useful *rule of thumb*, the strength of the three-phonon coupling will depend on the locality within the film, where the modes are propagating (and, of course, energy and momentum considerations).

We first consider the monolayer films. Within the Feynman approximation, we have calculated the dynamic structure function $S(q_\parallel,\omega)$ and the transition densities $\delta\rho(z;q_\parallel,\omega)$. For a complete discussion of the Feynman results, we refer the reader to paper II; our only intent here is to compare these with the corresponding quantities calculated in our more accurate CBF-BW calculation.

Figure 9 shows our results at a coverage of $n=0.065$ Å^{-2} in the Feynman approximation. This is close to the maximum coverage for which, at zero temperature, the film can still uniformly cover the substrate in the form of a monolayer. We have chosen this coverage since it displays already a strong ripplonlike excitation. The dotted line in the figure is the energy-momentum continuum boundary given by

$$\hbar\omega_{\rm cb}=-\mu+\frac{\hbar^2 q_\parallel^2}{2m}, \tag{3.1}$$

it separates regions, in energy-momentum space, where the modes are discrete from regions where the modes form a continuum. Here, μ is the chemical potential. The Feynman modes are strictly real, therefore we have broadened the discrete ones by 0.5 K, which is slightly less than the instrumental resolution of the neutron scattering experiments.[3] Figure 10 shows our results for the same coverage in the scaled CBF calculation. In both figures, one observes a clear phonon-maxon-roton signature, typical of bulk systems. The CBF calculation displays the expected effect of lowering the roton minimum significantly. This mode is essentially a two-dimensional phonon (called a layer phonon) and is longitudinally polarized. We also see the appearance of the ripplon (see discussion below), in both approximations. Now the ripplon has substantial spectral weight extending to long wavelengths. The ripplon level crosses at a momenta of approximately 1.4 Å^{-1}.

Comparing the Feynman and CBF-BW results, we find that the ripplon's energy is largely unaffected by three-phonon corrections. One can understand this result by considering the strength of the coupling between the Feynman modes. For momentum below 0.5 Å^{-1} only the Feynman ripplon has substantial spectral weight. Moreover, the transition densities[2] show that the ripplon and layer phonon have most of their strength located at different regions in the film; the ripplon propagates near the outer surface while the phonon is largely localized within the film. (This behavior is apparent in the CBF-BW transition densities, discussed below, as well.) Consequently, at these wavelengths, there is very little coordinate space overlap of these modes. This means that only ripplon-ripplon coupling will influence the amount, relative to the Feynman ripplon, by which the CBF-BW ripplon is renormalized.

The next relevant point follows from the approximately linear nature of the monolayer ripplon's dispersion. A discussion on scattering processes involving excitations having linear dispersion can be found, for example, in the text by Pines and Nozières.[26] In our case, we have in mind the process in which a ripplon of momentum $\mathbf{k}$ and energy $\omega(k)$ scatters, producing two other ripplon excitations of momenta $\mathbf{q}$ and $(\mathbf{k}-\mathbf{q})$, and energies $\omega(q)$ and $\omega(|\mathbf{k}-\mathbf{q}|)$. It then scatters back into the state with momentum $\mathbf{k}$ and energy $\omega(k)$. For this process, the total energy between scattering events will be

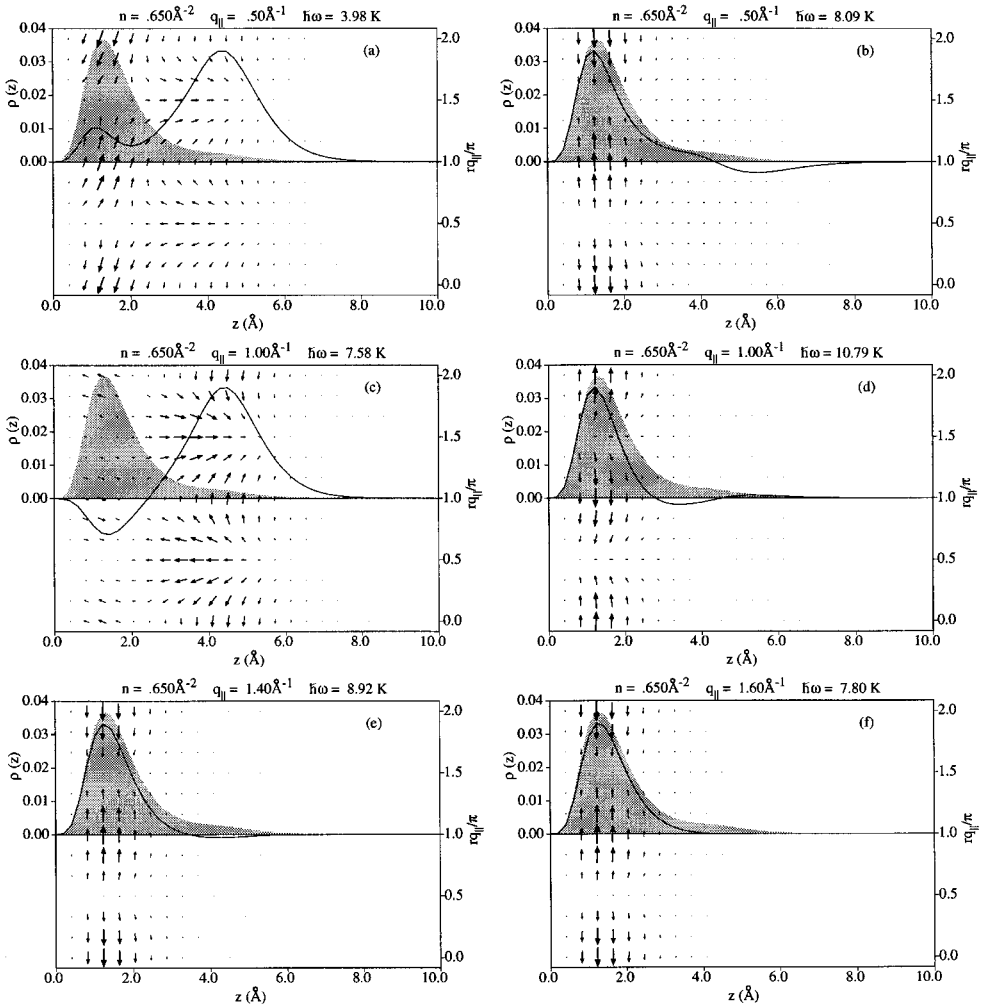

FIG. 11. The particle current in the CBF theory for a monolayer film with $n=0.065$ Å^{-2} as a function of wave number. The gray-shaded area depicts the background density, the solid line the transition density corresponding to the excitation, and the superimposed vector field is the particle current flow.

$$\omega=\omega(|\mathbf{k}-\mathbf{q}|)+\omega(|q|). \tag{3.2}$$

The important point, then, is that for linear dispersion, the only energy and momentum conserving processes are forward or backward scattering. This has the effect of severely limiting the phase space over which three-phonon scattering can occur. Thus one can understand the comparatively small ripplon renormalization, observed in Fig. 10, from these simple arguments.

Another important observation is that at momentum above 1.1 Å^{-1} the intensity of the ripplon is highly reduced. This broadening is due mainly to the decay of the ripplon into a long-wavelength ripplon and a layer roton. This effect will also be encountered at higher coverages.

Unlike the Feynman results, there now appears scattering intensity at a momentum $k>1.5$ Å^{-1} above 20 K. The energy of the peak is approximately the sum of the (Feynman) energies of the layer maxon and the layer roton. Consequently, the observed scattering intensity is easily traced to a large contribution to the two-body density of states coming from the hybridization of these two modes. This is basically a bulk effect that has also been observed in the three-dimensional liquids,[14] we find here the two-dimensional analog of this phenomenon. The effect is of no further concern for our discussion of excitations that are specific to the film geometry.

2. Particle currents and transition densities

The physical nature of individual excitations is best revealed in the *transition densities* and the *particle currents*. The reader is referred to Appendix D for a complete description of the theoretical current calculation. Again we mention the Feynman approximation only for comparison. Basically, we found that the CBF corrections [i.e., the second term in Eq. (B17)] do not, to any appreciable fashion, change the general flow patterns except, of course, for the shift in energy in particular in the roton region.

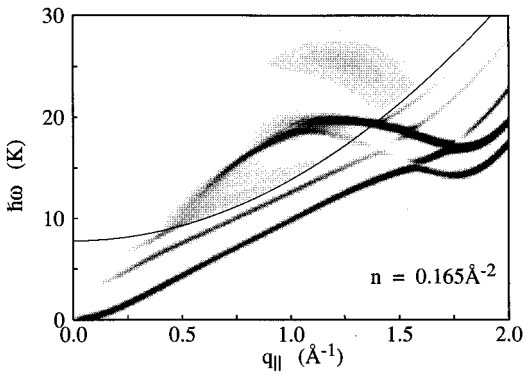

FIG. 12. The dynamic structure function in the Feynman approximation for the $n=0.165$ Å^2 film.

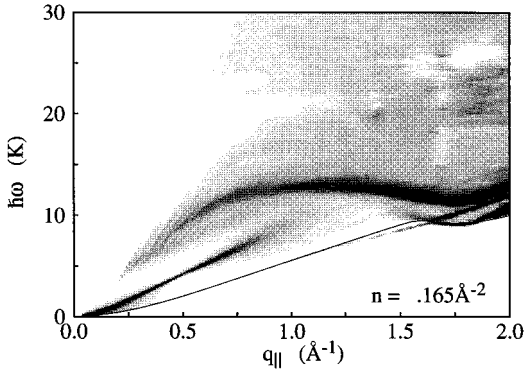

FIG. 13. The dynamic structure function in the scaled CBF approximation for the $n=0.165$ Å^2 film.

Figures 11(a)–11(f) show our results for transition densities and particle currents at a monolayer coverage of 0.065Å^{-2}. The density profile (grey-shaded region) and transition densities (solid lines) have been included in the figure as indicators of the location where the mode propagates. The arrows indicate the direction of the current parallel to the surface [as, for example, in Fig. 11(b)] and perpendicular to the surface [as in Fig. 11(a)].

Figure 11(a) shows the transition density and the particle current for the lowest excited state at the rather long wavelength of $k=0.5$ Å^{-1}. Obviously, the excitation propagates in the very low-density regime of the film, and the currents show the circular flow pattern typical for a ripplon. The next excitation [note that we use the term ''excitation'' in a somewhat loose sense, we refer to it as a peak in the $S(k,\omega)$] is, on the other hand, localized mostly within the layer and shows the longitudinal flow pattern of a phonon.

Figures 11(c) and 11(d) show basically the same situation at a somewhat larger momentum. Note that, while the lowest excitation is already rather diffuse, the ripplon character is clearly revealed in the current patterns shown in Fig. 11(c). At higher wave numbers, the ripplon loses most of its strength and the most visible resonance is the phonon-roton [Figs. 11(e) and 11(f)]. Note, however, that the ripplon still *can* be traced up to higher momentum transfers above the phonon-roton spectrum, however it is, as opposed to the Feynman approximation, very diffuse. Therefore, we call this a level crossing, as opposed to a level repulsion. In the later case the lowest-energy mode would still be the surface mode. We shall show, in the next sections, examples for the ripplon appearing above the roton minimum further below.

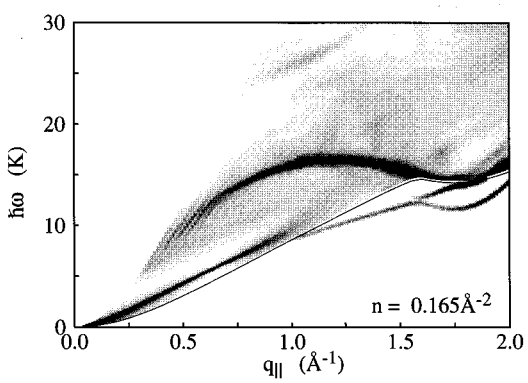

FIG. 14. The dynamic structure function in the unscaled CBF approximation for the $n=0.165$ Å^2 film.

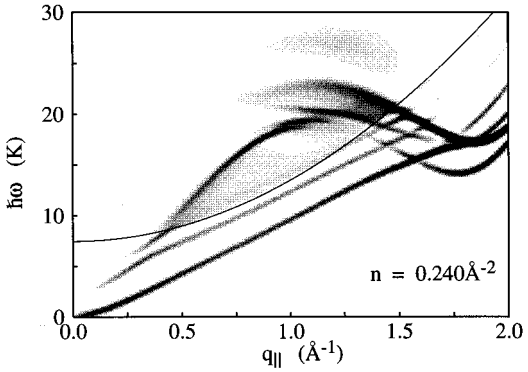

FIG. 15. The dynamic structure function in the Feynman approximation for the $n=0.240$ Å^{-2} film.

D. Multilayer films

1. Dynamic structure function

Let us now turn to our numerical results of the Feynman and CBF-BW theories for multilayer films. For the purpose of discussion, we have chosen two representative cases: a triple-layer film at 0.165 Å^{-2} and a four-layer film at 0.240 Å^{-2}. Figures 12 and 13 show the triple-layer film's dynamic structure function in the Feynman and the scaled CBF-BW approximation. Figure 14 shows, for comparison, the dynamics structure function in the ''unscaled'' version of the CBF-BF theory. The essential effect of the more realistic energy denominator used in the ''scaled'' approximation is that the continuum boundary and the modes at medium and short wavelengths ($q_\parallel > 0.5$ Å^{-1}) are moved to lower energies. This has the effect that the ripplon is, in the momentum regime 0.75 Å$^{-1} < q_{||} < 1.25$ Å^{-1}, hardly visible. Otherwise, the relative location and strengths of individual modes is essentially unaltered. Figures 15 and 16 show our results for the dynamic structure function at a coverage of 0.240 Å^{-2}. This coverage was chosen since the cleanest experimental data are available; the film consists of three complete and a fourth half-filled layer, cf. Fig. 1.

At both coverages one can see, in the Feynman results, a clear signature of two layer phonons, a ripplon, and another

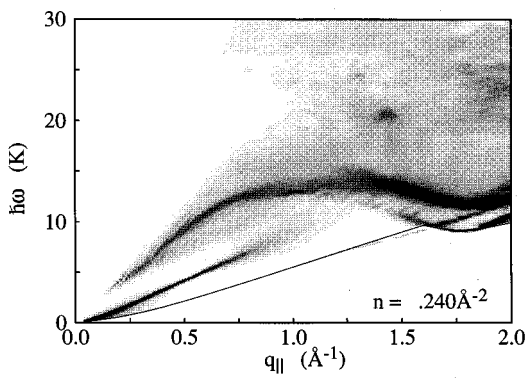

FIG. 16. The dynamic structure function in the scaled CBF approximation for the $n=0.240$ Å^{-2} film.

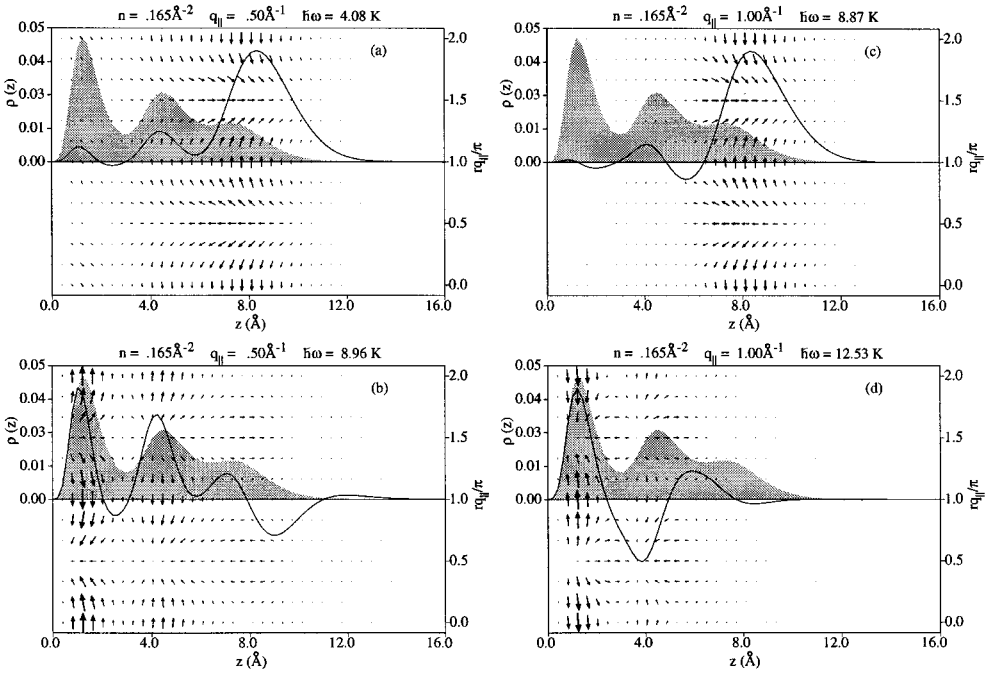

FIG. 17. The particle currents for the $n=0.165$ Å^{-2} film at long and intermediate wavelengths. See Fig. 11 for further explanations.

excitation of similar dispersion to the ripplon. In the CBF-BW theory we find, however, that the intermediate energy mode is highly damped. This is a manifestation of the fact that theories more sophisticated than the Feynman theory (such as the CBF-BW theory) contain mode coupling as an important ingredient. It is also consistent with experimental data in that the area between the ripplon and the phonon-roton spectrum is filled by a broad plateau. The accompanying paper, Ref. 3, will display the effect of filling the plateau more clearly in a different representation of the theoretical and experimental results for $S(q_\parallel,\omega)$.

Near the momentum $q_\parallel\approx 1.3$ Å^{-1} we find a second, less intense, layer mode (better described as a resonance) gaining significant spectral weight (see Fig. 16). At that momentum, which is between the maxon and roton, the intense layer phonon (the third resonance) is distributed over the two outer layers. This is the first case where modes having pronounced spectral weight encompassing multiple layers are becoming present in the film. (Support for these statements are given below.) The low-intensity mode (second-excited state) has a substantial amount of weight located at the film's inner layer at this momentum. At $q_\parallel\approx 2.0$ Å^{-1}, well above the level crossing, a mode with spectral weight distributed over the two outer layers is again obvious. Now, however, it is the second excited state. The lowest-energy state is the layer roton propagating in the first layer of the solid-liquid interface. The ripplon is the third-excited state.

2. Particle currents and transition densities

Some of the statements made above about the physical nature of individual resonances need to be substantiated by looking at *where* in the film the excitations are propagating, and what the particle motion is. Figures 17 and 18 show our results for the CBF currents, for selected wave numbers, at coverage of 0.165 Å^{-2} for the first two or three excitations. Figures 19 and 20 give the corresponding results for the four-layer film. In both cases, the lowest, long- to medium-wavelength excitations are ripplons — the transition density indicates that they propagate in the surface and the current shows the characteristic circular pattern. Note that, when considering the $S(q_\parallel,\omega)$, the ripplon is in fact quite diffuse and weak for a wave number of $q_\parallel\approx 1$Å^{-1}, nevertheless it can be clearly identified by its current patterns. The second excitation propagates mostly in the innermost layer, but, with increasing wavelength, has also a significant overlap with the outer layers of the film, note [cf. Figs. 17(b) and 20] that the transition density for wave number $q_\parallel=0.5$ Å^{-1} is almost in phase with the background density.

While the interpretation of long-wavelength results is relatively straightforward, the situation is more complicated in the vicinity of the roton minimum. Figures 18 and 20 show the particle currents for the three lowest pronounced resonances in that area. One of the resonances still displays some of the circular flow pattern of a ripplon, but there is less motion perpendicular to the surface. This resonance is the lowest mode at $q_\parallel\approx 1.5$ Å^{-1}, it reappears after the level crossing at $q_\parallel\approx 1.7$ Å^{-1} as the second resonance, whereas a layer-phonon propagating in the layer closest to the substrate is now the lowest mode. In both cases, the *third* resonance appears to be a mode that propagates with sizable probability throughout the whole film. We conjecture therefore that this mode will eventually develop into the bulk phonon-roton spectrum in the limit of infinite film thickness.

E. Comparison with neutron scattering experiments

Inelastic neutron scattering experiments on low temperature helium films have been performed at the time-of-flight spectrometer at the Insitut Laue-Langevin's reactor, and the resulting dynamic structure function from these experiments has been analyzed in an accompanying paper.[3] That work dealt with a four-layer film of coverage of 0.240 Å^{-2} which provided the motivation for us to use the same coverage here. In Ref. 3, the experimental aspects of the problem are stressed so here we concentrate on the theoretical explana-

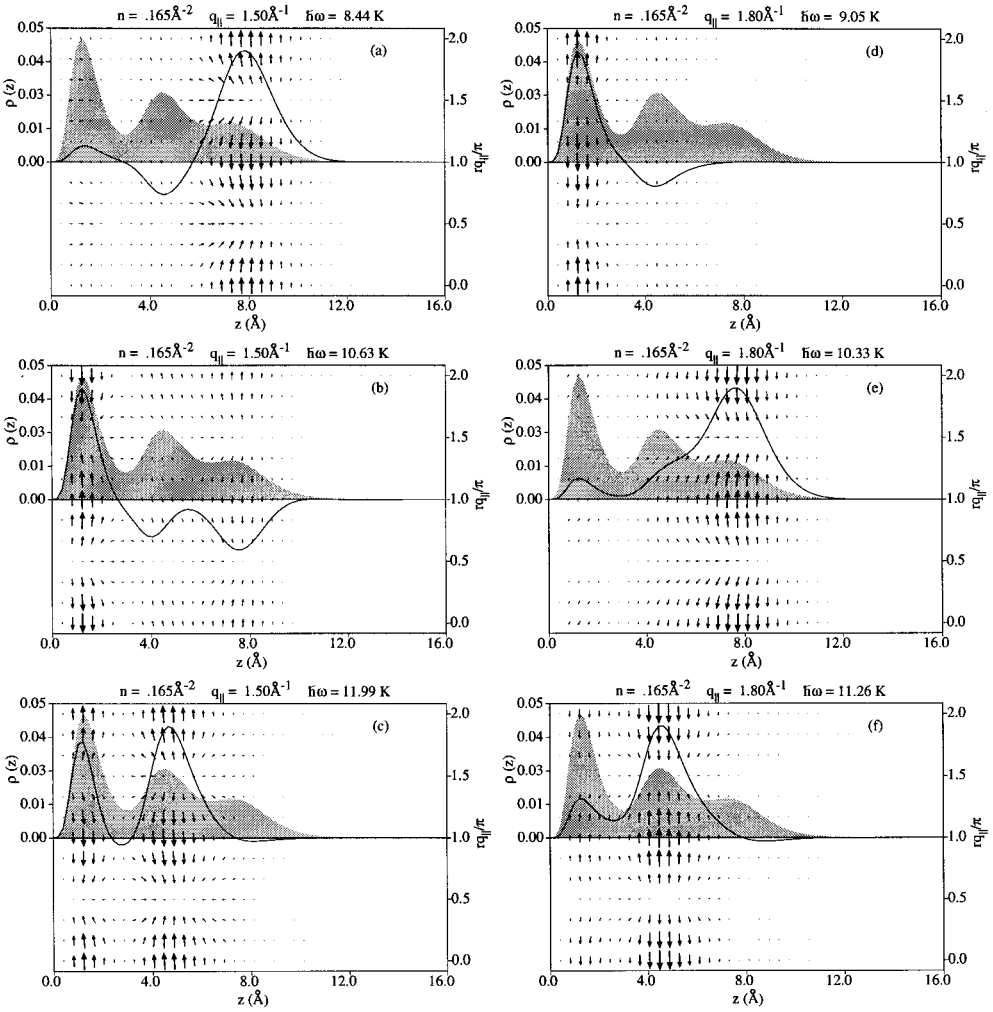

FIG. 18. The particle currents for the $n = 0.165$ Å^{-2} film in the vicinity of the roton mimimum and the level crossings. See Fig. 11 for further explanations.

tions. We proceed by first stating the experimental observation, and then use our theoretical results to explain it. In part, this section serves as a summary of some of the important findings of the previous sections.

First, the experimental ripplon has significant strength at low momenta, but appears to lose much of it at intermediate momenta. As already mentioned above, both the CBF-BW and scaled CBF-BW theories provide a clear explanation for this. At low momenta, only the ripplon has significant strength; at this coverage there is a sizable energy gap separating the higher energy modes; the theory finds these modes to have minimal strength. The argument for why the ripplon is largely undamped rests on the restricted phase space allowed by energy and momentum conservation for ripplon-ripplon scattering to take place. However, as the ripplon reaches an energy comparable to the layer roton, it can decay into a long-wavelength ripplon and a layer roton, for example, and thus damping is apparent.

Second, the experiment yields a strong mode that can be interpreted as the precursor to the bulk phonon-maxon roton. At the level of the Feynman theory of paper II, this observation was disturbing because it meant that the experimental results might be biased towards bulklike behavior. The cause was thought to be the helium condensation at the boarders of the graphite crystallites making up the scattering sample. The problem arose when the Feynman theory (Fig. 15), at that coverage, produced a clear, distinct set of layer modes (at the energy of the Feynman phonon-maxon roton) reflecting the layered nature of a *thin* film. The CBF-BW and, more so, the scaled CBF-BW theories help to resolve this. When mode coupling is included, we see immediately from Figs. 15 and 16 that the maxon-roton region of the excitation is enhanced. As already described above, this is a natural consequence of reducing the independence of the individual layer modes. In the corresponding transition densities, modes of large spectral weight distributed over considerable portions of the film — the signature of bulk coherence — now exist at those momenta and energies.

Third, the experiment finds a substantial plateau in the scattering intensity between the ripplon and bulklike mode. A theoretical explanation for this observation was already proposed in II, which invoked the obvious argument that the intermediate energy modes must account for the additional scattering intensity. In our more refined CBF theories we certainly see that this remains to be the proper explanation. Furthermore, scattering arising from hybridization of modes

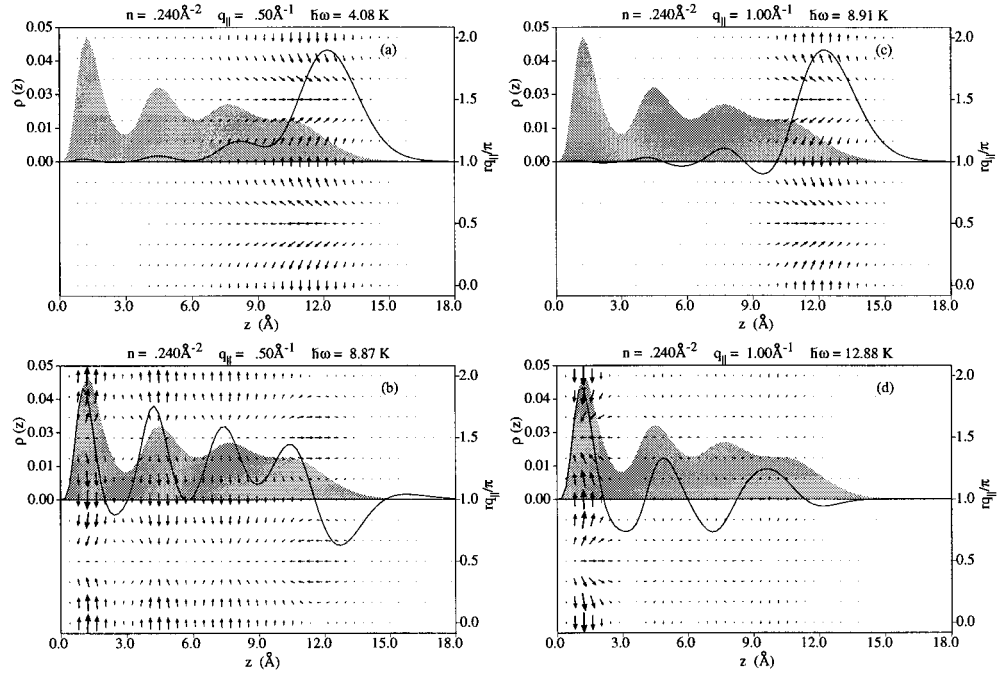

FIG. 19. The particle currents for the $n=0.240$ Å^{-2} film at long and intermediate wavelengths. See Fig. 11 for further explanations.

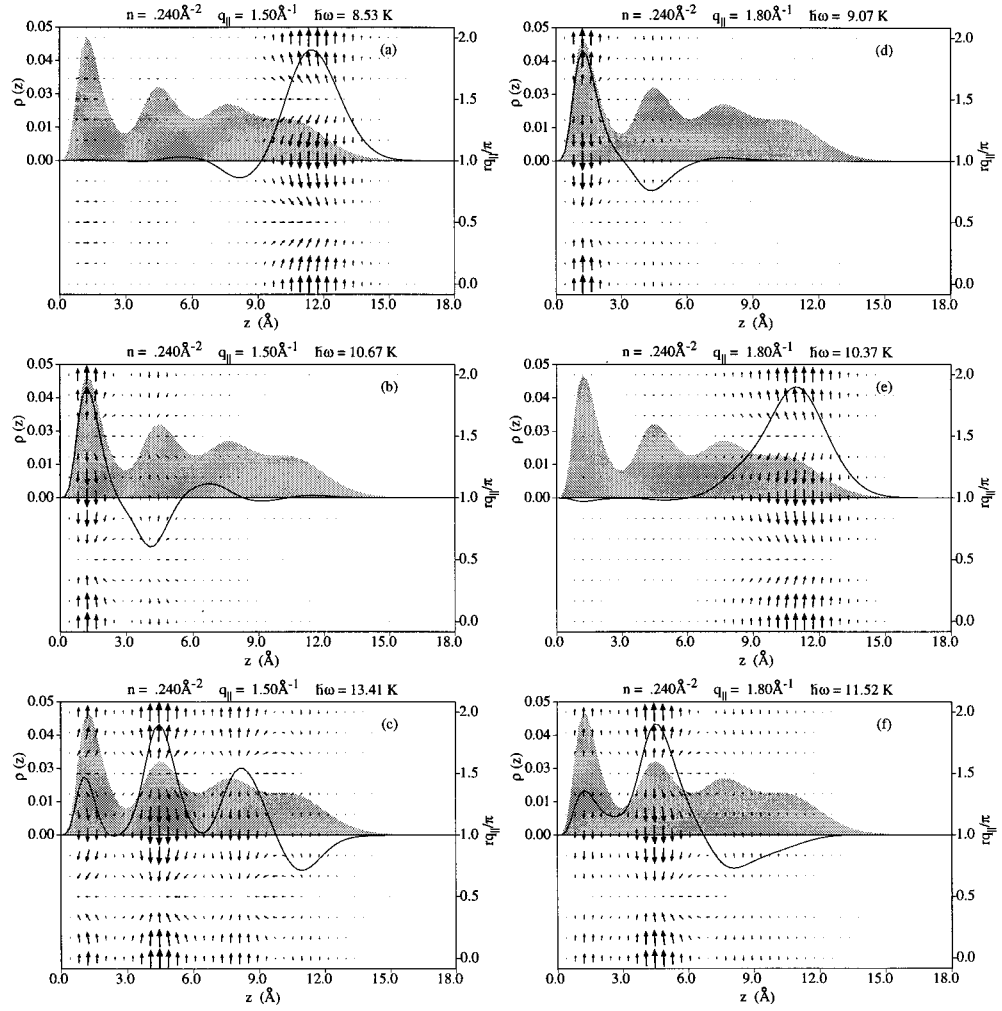

FIG. 20. The particle currents for $n=0.240$ Å^{-2} film in the vicinity of the roton minimum and the level crossings. See Fig. 11 for further explanations.

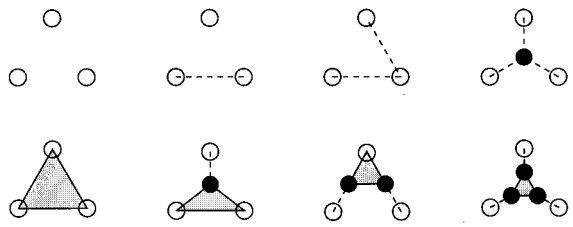

FIG. 21. The diagrammatic representation of the three-body distribution function $g(\mathbf{r}_1,\mathbf{r}_2,\mathbf{r}_3)$ in terms of pair distribution functions $h(\mathbf{r}_i,\mathbf{r}_j)=g(\mathbf{r}_i,\mathbf{r}_j)-1$ (solid lines) and an irreducible triplet function $X_3(\mathbf{r}_1,\mathbf{r}_2,\mathbf{r}_3)$ (shaded triangle).

occurs at these intermediate (and higher) energies adds to the background scattering intensity. Finally, multiphonon scattering processes are known to increase rapidly with temperature, and had we been able to take this into account, we might have recovered the full strength of the observed plateau.

IV. DISCUSSION AND SUMMARY

Most of our findings, theoretical ramifications, and comparisons with experiments, have been discussed in the preceding sections, there is no point for repetition. It appears that excitations that are, in essence, density fluctuations, specifically ''phononlike'' and ''ripplonline'' excitations, are well understood. The transition from the Feynman description to the CBF theory has added two new important qualitative features to the theory: mode-mode coupling and natural broadening. In many aspects, however, the qualitative picture derived from the Feynman theory has not changed. These are the specific types of modes (layer phonons, bulk phonons, and ripplons), their relative energetics, and their level crossings. Unfortunately, the *natural width* of our modes has turned out to be significantly smaller than the experimental width. We have gone through a very careful analysis of experimental data[3] and have concluded that there is indeed compelling experimental evidence that our overall picture of the dynamics of liquid films is a valid one.

This does not necessarily mean that nothing else can be learned from neutron scattering experiments on liquid films. We have stressed above that we believe that we have a good understanding of excitations that are essentially density fluctuations. However, there may be *other, new* types of excitations. These could, for example, be precritical phenomena to the liquid-solid phase transition in the highly compressed inner layers,[27] or vortex-type excitations.[28] In particular the ''flat'' modes found in low energy neutron scattering data[29,30] could be signatures of the latter. Neutron scattering experiments with a significantly improved energy resolution would be highly desirable since such experiments have the potential of pointing towards new physics beyond phonons, rotons, and ripplons.

ACKNOWLEDGMENTS

This work was supported, in part, by the National Science Foundation under Grant Nos. PHY-9108066 and DMR-9509743 (to E.K.) and by the North Atlantic Treaty Organization under Grant No. CRG 940127 (to E.K. and H. Lauter from the Institute Laue Langevin). B.E.C. and E.K. are grateful to the Institute Laue-Langevin, for partial support and for their kind hospitality. Discussions with G. Agnolet, C. E. Campbell, H. Godfrin, H. J. Lauter, P. Leiderer, P. Nozières, M. Saarela, and W. M. Saslow are gratefully acknowledged. Computational resources were provided by the Texas High Performance Computing Center. We also thank S. Moroni, D. Ceperley, and G. Senatore for communication of unpublished data (Ref. 24).

APPENDIX A: EQUATIONS OF MOTION

We start our considerations with the Lagrangian (2.3)

$$\begin{aligned}\mathscr{L}(t)=&\frac{1}{8}\langle\Psi_0|[\,\delta U^*,[T,\delta U]]|\Psi_0\rangle\\&-\frac{i\hbar}{8}\Big[\Big\langle\Psi_0\Big|\,\delta\dot{U}[\,\delta U^*\\&-\langle\Psi_0|\,\delta U^*|\Psi_0\rangle]\,\Big|\Psi_0\Big\rangle-\text{c.c.}\Big]\\&+\Big\langle\Psi_0(t)\Big|\sum_i U_{\text{ext}}(\mathbf{r}_i;t)\Big|\Psi_0(t)\Big\rangle.\end{aligned}\tag{A1}$$

For the derivation of the double-commutator term in the above equation, one normally assumes that $|\Psi_0\rangle$ is the exact ground state. However, for the specific form (2.1) of the excitation operator, it is sufficient to assume that the correlations up to u_4 have been optimized. Inserting the explicit form of our time-dependent correlations allows us to rewrite the double-commutator term in terms of one-, two-, and three-body densities:

$$\begin{aligned}\frac{1}{8}\langle\Psi_0|[\,\delta U^*,[T,\delta U]]|\Psi_0\rangle=\frac{\hbar^2}{8m}\Big\{&\int d^3r\rho_1(\mathbf{r})|\nabla\delta u_1(\mathbf{r};t)|^2+\int d^3r_1d^3r_2\rho_2(\mathbf{r}_1,\mathbf{r}_2)[\nabla_1\delta u_1(\mathbf{r_1};t)\cdot\nabla_1\delta u_2^*(\mathbf{r}_1,\mathbf{r}_2;t)+\text{c.c.}\\&+|\nabla_1\delta u_2\mathbf{r}_1,\mathbf{r}_2;t)|^2]+\int d^3r_1d^3r_2d^3r_3\rho_3(\mathbf{r}_1,\mathbf{r}_2,\mathbf{r}_3)\nabla_1\delta u_2(\mathbf{r}_1,\mathbf{r}_2)\nabla_1\delta u_2^*(\mathbf{r}_1,\mathbf{r}_2)\Big\}.\end{aligned}\tag{A2}$$

The time-derivative term is conveniently expressed in terms of (time derivatives of) the time-dependent one- and two-body densities $\delta\rho_1(\mathbf{r};t)$ and $\delta\rho_2(\mathbf{r}_i,\mathbf{r}_j;t)$ to be taken to first order in the fluctuations:

$$\Big\langle\Psi_0\Big|\,\delta\dot{U}[\,\delta U^*-\langle\Psi_0|\,\delta U^*|\Psi_0\rangle]\,\Big|\Psi_0\Big\rangle=\int d^3r\dot{\rho}_1(\mathbf{r};t)\,\delta u_1^*(\mathbf{r};t)+\frac{1}{2}\int d^3r_1d^3r_2\dot{\rho}_2(\mathbf{r}_1,\mathbf{r}_2;t)\,\delta u_2^*(\mathbf{r}_1,\mathbf{r}_2;t).\tag{A3}$$

A word is in order concerning the interpretation of the time derivative of the above densities: These are *not* the time derivatives of the (real) physical density, but rather should be understood as an abbreviation of the operation

$$\dot{\rho}_1(\mathbf{r}_1;t)\equiv\int d^3r_2\left[\frac{\delta\rho_1(\mathbf{r}_1)}{\delta u_1(\mathbf{r}_2)}\right]\delta\dot{u}_1(\mathbf{r}_2;t)+\int d^3r_2d^3r_3\left[\frac{\delta\rho_1(\mathbf{r}_1)}{\delta u_2(\mathbf{r}_2,\mathbf{r}_3)}\right]\delta\dot{u}_2(\mathbf{r}_2,\mathbf{r}_3;t) \tag{A4}$$

and a corresponding equation for the time-dependent pair density. In other words, $\dot{\rho}_1(\mathbf{r}_1)$ and $\dot{\rho}_2(\mathbf{r}_1,\mathbf{r}_2)$ are *complex*. The physical time-dependent densities are obtained by taking the real part of these functions.

Finally, we calculate the term containing the external field to first order in the fluctuations

$$\begin{aligned}\int d^3r\,\mathrm{Re}\rho_1(\mathbf{r};t)U_{\mathrm{ext}}(\mathbf{r};t)=\mathrm{Re}\Bigg\{&\int d^3r_1U_{\mathrm{ext}}(\mathbf{r}_1;t)\Bigg[\rho_1(\mathbf{r}_1)\delta u_1(\mathbf{r}_1;t)+\int d^3r_2[\rho_2(\mathbf{r}_1,\mathbf{r}_2)-\rho_1(\mathbf{r}_1)\rho_1(\mathbf{r}_2)]\delta u_1(\mathbf{r}_2;t)\Bigg]\\&+\frac{1}{2}\int d^3r_1d^3r_2[U_{\mathrm{ext}}(\mathbf{r}_1;t)+U_{\mathrm{ext}}(\mathbf{r}_2;t)]\rho_2(\mathbf{r}_1,\mathbf{r}_2)+\frac{1}{2}\int d^3r_1d^3r_2d^3r_3U_{\mathrm{ext}}(\mathbf{r}_3;t)[\rho_3(\mathbf{r}_1,\mathbf{r}_2,\mathbf{r}_3)\\&-\rho_1(\mathbf{r}_3)\rho_2(\mathbf{r}_1,\mathbf{r}_2)]\delta u_2(\mathbf{r}_1,\mathbf{r}_2;t)\Bigg\}.\end{aligned} \tag{A5}$$

Taking the variations of the second-order functional leads to two EOM's of the form

$$\begin{aligned}&\frac{\hbar^2}{2m}\nabla_1\cdot\Bigg\{\rho_1(\mathbf{r}_1)\nabla_1\delta u_1(\mathbf{r}_1;t)+\int d^3r_2\rho_2(\mathbf{r}_1,\mathbf{r}_2)\nabla_1\delta u_2(\mathbf{r}_1,\mathbf{r}_2;t)\Bigg\}\\&\quad=-i\hbar\dot{\rho}_1(\mathbf{r}_1;t)+2\Bigg\{\rho_1(\mathbf{r}_1)U_{\mathrm{ext}}(\mathbf{r}_1;t)+\int d^3r_2[\rho_2(\mathbf{r}_1,\mathbf{r}_2)-\rho_1(\mathbf{r}_1)\rho_1(\mathbf{r}_2)]U_{\mathrm{ext}}(\mathbf{r}_2;t)\Bigg\}\end{aligned} \tag{A6}$$

and

$$\begin{aligned}&\frac{\hbar^2}{2m}\nabla_1\cdot\Bigg\{\rho_2(\mathbf{r}_1,\mathbf{r}_2)\nabla_1\delta u_1(\mathbf{r}_1;t)+\rho_2(\mathbf{r}_1,\mathbf{r}_2)\nabla_1\delta u_2(\mathbf{r}_2,\mathbf{r}_2;t)+\int d^3r_3\rho_3(\mathbf{r}_1,\mathbf{r}_2,\mathbf{r}_3)\nabla_1\delta u_2(\mathbf{r}_1,\mathbf{r}_3;t)\Bigg\}+\text{same for }(1\leftrightarrow2)\\&\quad=-i\hbar\dot{\rho}_2(\mathbf{r}_1,\mathbf{r}_2;t)+2\rho_2(\mathbf{r}_1,\mathbf{r}_2)[U_{\mathrm{ext}}(\mathbf{r}_3;t)+U_{\mathrm{ext}}(\mathbf{r}_3;t)]+2\int d^3r_3[\rho_3(\mathbf{r}_1,\mathbf{r}_2,\mathbf{r}_3)-\rho_2(\mathbf{r}_1,\mathbf{r}_2)\rho_1(\mathbf{r}_3)]U_{\mathrm{ext}}(\mathbf{r}_3;t).\end{aligned} \tag{A7}$$

Equations (A6) and (A7) are the starting point for the equations-of-motion method for the calculation of collective excitations in quantum liquids. Different implementations[12,5,6,31] differ by the approximations used for the three- and four-body densities appearing in the equations of motion and the time derivative of one- and two-body densities. An important consideration is that the one- and the two-body equations are *not* independent: The one-body equation (1.6) results from the two-body equation in the limit $|\mathbf{r}_1-\mathbf{r}_2|\to\infty$. Moreover, using the sequential relations

$$\int d^3r_n\rho_n(\mathbf{r}_1,\ldots,\mathbf{r}_n)=(N-n)\rho_n(\mathbf{r}_1,\ldots,\mathbf{r}_n) \tag{A8}$$

it is easily seen that the one-body equation also results when Eq. (A7) is integrated over one coordinate, say, $\mathbf{r}_2$. In order to decouple the two equations, we first subtract the asymptotic limit, multiplied by $g(\mathbf{r}_1,\mathbf{r}_2)$. At the same time, the equations can be shortened considerably by introducing the one-body current

$$-i\mathbf{j}(\mathbf{r};t)=\frac{\hbar\rho_1(\mathbf{r})}{2m}\Bigg\{\nabla\delta u_1(\mathbf{r};t)+\int d^3r'\rho_1(\mathbf{r}')g(\mathbf{r},\mathbf{r}')\nabla\delta u_2(\mathbf{r},\mathbf{r}';t)\Bigg\}. \tag{A9}$$

The one-body equation is then readily identified with the continuity equation,

$$i\hbar[\nabla\cdot\mathbf{j}(\mathbf{r};t)-\dot{\rho}_1(\mathbf{r};t)]+2\rho_1(\mathbf{r})\Bigg[U_{\mathrm{ext}}(\mathbf{r};t)+\int d^3r'\rho_1(\mathbf{r}')h(\mathbf{r},\mathbf{r}')U_{\mathrm{ext}}(\mathbf{r}';t)\Bigg]=0, \tag{A10}$$

where $h(\mathbf{r},\mathbf{r}')\equiv g(\mathbf{r},\mathbf{r}')-1$, and the two-body equation becomes

$$\begin{aligned}&\frac{\hbar^2}{2m}\frac{1}{\rho_1(\mathbf{r}_1)}\nabla_1\rho_1(\mathbf{r}_1)\cdot\Bigg\{g(\mathbf{r}_1,\mathbf{r}_2)\nabla_1\delta u_2(\mathbf{r}_1,\mathbf{r}_2)+\int d^3r_3\rho_1(\mathbf{r}_3)[g_3(\mathbf{r}_1,\mathbf{r}_2,\mathbf{r}_3)-g(\mathbf{r}_1,\mathbf{r}_3)g(\mathbf{r}_1,\mathbf{r}_2)]\nabla_1\delta u_2(\mathbf{r}_1,\mathbf{r}_3;t)\Bigg\}\\&\quad+\text{same for }(1\leftrightarrow2)+i\hbar\dot{g}(\mathbf{r}_1,\mathbf{r}_2)=i\hbar\left[\frac{\mathbf{j}(\mathbf{r}_1)}{\rho_1(\mathbf{r}_1)}\cdot\nabla_1g(\mathbf{r}_1,\mathbf{r}_2)+\frac{\mathbf{j}(\mathbf{r}_2)}{\rho_1(\mathbf{r}_2)}\cdot\nabla_2g(\mathbf{r}_1,\mathbf{r}_2)\right]+2\int d^3r_3\rho_1(\mathbf{r}_3)\{g_3(\mathbf{r}_1,\mathbf{r}_2,\mathbf{r}_3)\\&\quad-g(\mathbf{r}_1,\mathbf{r}_2)[g(\mathbf{r}_1,\mathbf{r}_3)+g(\mathbf{r}_2,\mathbf{r}_3)-1]\}U_{\mathrm{ext}}(\mathbf{r}_3;t).\end{aligned} \tag{A11}$$

Before we turn to approximations, we carry out a cumulant analysis of the three-body distribution function. Using the usual diagrammatic notation, this cumulant expansion is shown in Fig. 21. In this figure, the solid line represents a function $h(\mathbf{r}_1,\mathbf{r}_2)$ and the shaded triangle is the part $X_3(\mathbf{r}_1,\mathbf{r}_2,\mathbf{r}_3)$ of the three-body distribution function that is non-nodal in all three external points. We also abbreviate the part of $g_3(\mathbf{r}_1,\mathbf{r}_2,\mathbf{r}_3)$ that is non-nodal in point $\mathbf{r}_3$ by

$$Y(\mathbf{r}_1,\mathbf{r}_2;\mathbf{r}_3)=h(\mathbf{r}_1,\mathbf{r}_3)h(\mathbf{r}_2,\mathbf{r}_3)+\int d^3r_4d^3r_5[\,\delta(\mathbf{r}_1-\mathbf{r}_4)+\rho_1(\mathbf{r}_4)h(\mathbf{r}_4,\mathbf{r}_1)][\,\delta(\mathbf{r}_2-\mathbf{r}_5)+\rho_1(\mathbf{r}_5)h(\mathbf{r}_5,\mathbf{r}_2)]X_3(\mathbf{r}_4,\mathbf{r}_5,\mathbf{r}_3). \tag{A12}$$

Finally, we change the independent one-body function from $\delta u_1(\mathbf{r};t)$ to $\delta\rho_1(\mathbf{r};t)$ For this purpose, we express the functional derivatives of the densities occurring in Eq. (A4) through two- and three-body densities,

$$\delta\rho_1(\mathbf{r};t)=\Big\{\rho_1(\mathbf{r}_1)\,\delta\delta u_1(\mathbf{r}_1;t)+\int d^3r_2[\rho_2(\mathbf{r}_1,\mathbf{r}_2)-\rho_1(\mathbf{r}_1)\rho_1(\mathbf{r}_2)]\delta u_1(\mathbf{r}_2;t)+\int d^3r_2\rho_2(\mathbf{r}_1,\mathbf{r}_2)\,\delta u_2(\mathbf{r}_1,\mathbf{r}_2;t)$$
$$+\frac{1}{2}\int d^3r_2d^3r_3[\rho_3(\mathbf{r}_1,\mathbf{r}_2,\mathbf{r}_3)-\rho_1(\mathbf{r}_3)\rho_2(\mathbf{r}_1,\mathbf{r}_2)]\,\delta u_2(\mathbf{r}_2,\mathbf{r}_3;t)\Big\}. \tag{A13}$$

Inserting the cumulant expansion of Fig. 21 for the three-body and defining

$$\delta v_1(\mathbf{r}_1;t)=\rho_1(\mathbf{r}_2)\,\delta u_1(\mathbf{r}_1;t)+\int d^3r_2\rho_2(\mathbf{r}_1,\mathbf{r}_2)\,\delta u_2(\mathbf{r}_1,\mathbf{r}_2;t)+\frac{1}{2}\int d^3r_2d^3r_3\rho_1(\mathbf{r}_2)\rho_1(\mathbf{r}_3)Y(\mathbf{r}_2,\mathbf{r}_3,\mathbf{r}_1)\,\delta u_2(\mathbf{r}_2,\mathbf{r}_3;t), \tag{A14}$$

let us rewrite $\delta\rho_1(\mathbf{r};t)$ as

$$\delta\rho_1(\mathbf{r};t)=\rho_1(\mathbf{r}_1)\Big[\,\delta v_1(\mathbf{r}_1;t)+\int d^3r_2h(\mathbf{r}_1,\mathbf{r}_2)\rho_1(\mathbf{r}_2)\,\delta v_1(\mathbf{r}_2;t)\Big] \tag{A15}$$

which is readily solved for $\delta v_1(\mathbf{r}_1;t)$ by inverting the convolution integral in Eq. (A15):

$$\rho_1(\mathbf{r}_1)\,\delta v_1(\mathbf{r}_1;t)=\delta\rho_1(\mathbf{r};t)-\int d^3r_2X(\mathbf{r}_1,\mathbf{r}_2)\,\delta\rho_1(\mathbf{r}_2;t), \tag{A16}$$

where $X(\mathbf{r}_1,\mathbf{r}_2)$ is the ''direct correlation function.'' The change of variables is useful since the HNC equations provide a relationship between $g(\mathbf{r}_1,\mathbf{r}_2)$, $u_2(\mathbf{r}_1,\mathbf{r}_2)$, and $\rho_1(\mathbf{r})$ in which $u_1(\mathbf{r})$ does not appear. In other words, we can from now on consider $\delta\rho_1(\mathbf{r};t)$ and $\delta u_2(\mathbf{r}_1,\mathbf{r}_2;t)$ as the independent variables. The time derivative of the two-body distribution function can then be written as

$$\dot g(\mathbf{r}_1,\mathbf{r}_2)=\int d^3r_3\frac{\delta g(\mathbf{r}_1,\mathbf{r}_2)}{\delta\rho_1(\mathbf{r}_3)}\,\delta\dot\rho_1(\mathbf{r}_3;t)+\int d^3r_3d^3r_4\frac{\delta g(\mathbf{r}_1,\mathbf{r}_2)}{\delta u_2(\mathbf{r}_3,\mathbf{r}_4)}\,\delta\dot u_2(\mathbf{r}_3,\mathbf{r}_4)\equiv\int d^3r_3Y(\mathbf{r}_1,\mathbf{r}_2;\mathbf{r}_3)\,\delta\dot\rho_1(\mathbf{r}_3;t)+\frac{\partial_u}{\partial t}g(\mathbf{r}_1,\mathbf{r}_2), \tag{A17}$$

where the first term in the last line is a definition of the operation ∂_u, and the first term again stems from graphical analysis.

$$\frac{\hbar^2}{2m}\frac{1}{\rho_1(\mathbf{r}_1)}\nabla_1\rho_1(\mathbf{r}_1)\cdot\Big\{g(\mathbf{r}_1,\mathbf{r}_2)\nabla_1\delta u_2(\mathbf{r}_1,\mathbf{r}_2)+\int d^3r_3\rho_1(\mathbf{r}_3)[g_3(\mathbf{r}_1,\mathbf{r}_2,\mathbf{r}_3)-g(\mathbf{r}_1,\mathbf{r}_3)g(\mathbf{r}_1,\mathbf{r}_2)]\nabla_1\delta u_2(\mathbf{r}_1,\mathbf{r}_3;t)\Big\}$$
$$+\text{same for }(1\leftrightarrow2)+i\hbar\frac{\partial_u}{\partial t}g(\mathbf{r}_1,\mathbf{r}_2;t)=i\hbar\Big[\frac{\mathbf{j}(\mathbf{r}_1)}{\rho_1(\mathbf{r}_1)}\cdot\nabla_1g(\mathbf{r}_1,\mathbf{r}_2)+\frac{\mathbf{j}(\mathbf{r}_2)}{\rho_1(\mathbf{r}_2)}\cdot\nabla_2g(\mathbf{r}_1,\mathbf{r}_2)-\int d^3r_3Y(\mathbf{r}_1,\mathbf{r}_2;\mathbf{r}_3)\nabla\cdot\mathbf{j}(\mathbf{r}_3)\Big]. \tag{A18}$$

The equation still satisfies a sequential relation: Observing that

$$\int d^3r_2[g_3(\mathbf{r}_1,\mathbf{r}_2,\mathbf{r}_3)-g(\mathbf{r}_1,\mathbf{r}_2)g(\mathbf{r}_1,\mathbf{r}_3)]\rho_1(\mathbf{r}_2)=-g(\mathbf{r}_1,\mathbf{r}_3) \tag{A19}$$

and

$$\int d^3r_2\rho_1(\mathbf{r}_2)Y(\mathbf{r}_1,\mathbf{r}_2;\mathbf{r}_3)=-h(\mathbf{r}_1,\mathbf{r}_3) \tag{A20}$$

it is readily shown that volume integral of *both* sides of the equation of motion (A18) vanishes. The advantage of the present formulation is that this is true for *any* triplet function $X_3(\mathbf{r}_1,\mathbf{r}_2,\mathbf{r}_3)$.

The interesting feature of the equation of motion (A18) is that the external potential has been eliminated. Evidently, the time dependence of the *pair correlations* is driven by the one-body current alone. Thus it is appropriate to identify the equations of

motion method with a *systematic* approach to introduce current-current coupling effects into the theory of excitations. Note that we have at this point made no approximations other than assuming that the time dependence of the wave function is described appropriately by a one-body and a two-body component.

The current then reads, in these variables,

$$-i\mathbf{j}(\mathbf{r}_1)=\frac{\hbar\rho_1(\mathbf{r}_1)}{2m}\nabla_1\left[\frac{\delta\rho_1(\mathbf{r}_1;t)}{\rho_1(\mathbf{r}_1;t)}-\int d^3r_2X(\mathbf{r}_1,\mathbf{r}_2)\delta\rho_1(\mathbf{r}_2;t)\right]+\frac{\hbar\rho_1(\mathbf{r}_1)}{2m}\int d^3r_2\rho_1(\mathbf{r}_2)\delta u_2(\mathbf{r}_1,\mathbf{r}_2;t)\nabla_1 g(\mathbf{r}_1,\mathbf{r}_2)$$
$$+\frac{\hbar\rho_1(\mathbf{r}_1)}{4m}\nabla_1\int d^3r_2d^3r_3\rho_1(\mathbf{r}_2)\rho_1(\mathbf{r}_3)Y(\mathbf{r}_2,\mathbf{r}_3,\mathbf{r}_1)\delta u_2(\mathbf{r}_2,\mathbf{r}_3;t) \tag{A21}$$

and the continuity equation is, when written in these variables,

$$i\hbar\dot{\rho}_1(\mathbf{r};t)=-\frac{\hbar^2}{2m}\nabla_1\left\{\rho_1(\mathbf{r}_1)\nabla\left[\frac{\delta\rho_1(\mathbf{r}_1;t)}{\rho_1(\mathbf{r}_1;t)}-\int d^3rX(\mathbf{r}_1,\mathbf{r}_2)\delta\rho_1(\mathbf{r}_2;t)\right]\right\}$$
$$-\frac{\hbar^2}{2m}\nabla_1\left[\rho_1(\mathbf{r}_1)\int d^3r_2\rho_1(\mathbf{r}_2)\delta u_2(\mathbf{r}_1,\mathbf{r}_2;t)\nabla_1 g(\mathbf{r}_1,\mathbf{r}_2)\right]$$
$$-\frac{\hbar^2}{4m}\nabla_1\left[\rho_1(\mathbf{r}_1)\nabla_1\int d^3r_2d^3r_3\rho_1(\mathbf{r}_2)\rho_1(\mathbf{r}_3)Y(\mathbf{r}_2,\mathbf{r}_3,\mathbf{r}_1)\delta u_2(\mathbf{r}_2,\mathbf{r}_3;t)\right]$$
$$+2\rho_1(\mathbf{r}_1)\left[U_{\rm ext}(\mathbf{r}_1;t)+\int d^3r_2\rho_1(\mathbf{r}_2)h(\mathbf{r}_1,\mathbf{r}_2)U_{\rm ext}(\mathbf{r}_2;t)\right]. \tag{A22}$$

The Feynman theory is recovered, from this form, by omitting the second and the third line of Eq. (A22).

APPENDIX B: CONVOLUTION APPROXIMATION

We now need to make a specific approximation to all the three-body or distribution functions and densities, as well as for the connection between the fluctuating pair correlation function to the time-dependent part of the two-body distribution functions. We will refer to the approximation scheme we have chosen as the convolution approximation since it is diagrammatically equivalent to the approximation used by Chang and Campbell[12] for the bulk system. The approximation is equivalent to the ''uniform limit'' approximation[32] which assumes that the two-body quantities under consideration are small in coordinate space, but not necessarily small in momentum space. This allows for long-range effects like phonons.

It is useful to introduce the tilde notation, for example for any one-body function $f_1(\mathbf{r})$ we define

$$\widetilde{f}_1(\mathbf{r})\equiv\sqrt{\rho_1(\mathbf{r})}f_1(\mathbf{r}), \tag{B1}$$

for a two-body function $f_2(\mathbf{r},\mathbf{r}')$ we define

$$\widetilde{f}_2(\mathbf{r},\mathbf{r}')\equiv\sqrt{\rho_1(\mathbf{r})\rho_1(\mathbf{r}')}f_2(\mathbf{r},\mathbf{r}'), \tag{B2}$$

and for the current

$$\widetilde{\mathbf{j}}(\mathbf{r})\equiv\frac{\mathbf{j}(\mathbf{r})}{\sqrt{\rho_1(\mathbf{r})}}. \tag{B3}$$

It is also useful to abbreviate the convolution product of a pair of two-body functions $\widetilde{A}(\mathbf{r},\mathbf{r}')$ and $\widetilde{B}(\mathbf{r},\mathbf{r}')$ as

$$[\widetilde{A}*\widetilde{B}](\mathbf{r},\mathbf{r}')\equiv\int d^3r''\widetilde{A}(\mathbf{r},\mathbf{r}'')\widetilde{B}(\mathbf{r}'',\mathbf{r}'). \tag{B4}$$

Besides the Feynman states $\psi^{(n)}(\mathbf{r})$ and their adjoints $\phi^{(n)}(\mathbf{r})$, we will also need the abbreviations

$$\zeta^{(n)}(\mathbf{r}_1)=\frac{\phi^{(n)}(\mathbf{r}_1)-\psi^{(n)}(\mathbf{r}_1)}{\sqrt{\rho_1(\mathbf{r}_1)}} \tag{B5}$$

and

$$\xi^{(n)}(\mathbf{r}_1)=\sqrt{\rho_1(\mathbf{r}_1)}\phi^{(n)}(\mathbf{r}_1). \tag{B6}$$

In keeping with the philosophy of the ''uniform limit approximation,'' we first rewrite the time-dependent pair correlation function in terms of the time dependence of the ''non-nodal'' function $X(\mathbf{r}_1,\mathbf{r}_2;t)$:

$$\frac{\partial_u\delta\widetilde{g}(\mathbf{r}_1,\mathbf{r}_2;t)}{\partial t}=\left[S*\frac{\partial_u\delta\widetilde{X}}{\partial t}*S\right](\mathbf{r}_1,\mathbf{r}_2;t). \tag{B7}$$

Two simplifications of the equations are made on the left-hand side of Eq. (A18): We approximate

$$g(\mathbf{r}_1,\mathbf{r}_2)\nabla_1\delta u_2(\mathbf{r}_1,\mathbf{r}_2;t)\approx\nabla_1\delta u_2(\mathbf{r}_1,\mathbf{r}_2;t)\approx\nabla_1\delta X(\mathbf{r}_1,\mathbf{r}_2;t) \tag{B8}$$

and the three-body term as

$$\int d^3r_3\rho_1(\mathbf{r}_3)[g_3(\mathbf{r}_1,\mathbf{r}_2,\mathbf{r}_3)-g(\mathbf{r}_1,\mathbf{r}_3)g(\mathbf{r}_1,\mathbf{r}_2)]\nabla_1\delta u_2(\mathbf{r}_1,\mathbf{r}_3;t)\approx\int d^3r_3\rho_1(\mathbf{r}_3)\nabla_1\delta u_2(\mathbf{r}_1,\mathbf{r}_3;t)h(\mathbf{r}_3,\mathbf{r}_2)$$

$$\approx\int d^3r_3\rho_1(\mathbf{r}_3)\nabla_1\delta X(\mathbf{r}_1,\mathbf{r}_3;t)h(\mathbf{r}_3,\mathbf{r}_2). \tag{B9}$$

This approximation is actually less dramatic as it may seem at the first glance; a careful diagrammatic analysis of the three-body distribution function shows that, by expressing $\delta u_2(\mathbf{r}_1,\mathbf{r}_3;t)$ in terms of $\delta X(\mathbf{r}_1,\mathbf{r}_3;t)$, a large number of diagrams are eliminated that would contribute if one worked in terms of $\delta u_2(\mathbf{r}_1,\mathbf{r}_3;t)$. Unfortunately, a complete elimination of $\delta u_2(\mathbf{r}_1,\mathbf{r}_3;t)$ in favor of either $\delta X(\mathbf{r}_1,\mathbf{r}_3;t)$ or $\delta g(\mathbf{r}_1,\mathbf{r}_3;t)$ on the left-hand side of the EOM does not lead to any simplifications and appears to be impractical for the nonuniform geometry. Finally, we use for the triplet function $X_3(\mathbf{r}_1,\mathbf{r}_2,\mathbf{r}_3)$ the expression obtained in paper I from the optimization of the triplet correlations.

From here on, it is advantageous to work entirely in the space defined by the Feynman wave functions and to express the one- and two-body fluctuations as

$$\frac{\delta\rho_1(\mathbf{r};t)}{\sqrt{\rho_1(\mathbf{r})}}=\sum_m r_m(t)\phi^{(m)}(\mathbf{r}),$$

$$\delta\widetilde{X}(\mathbf{r}_1,\mathbf{r}_2;t)=\sum_{mn} X_{mn}(t)\psi^{(m)}(\mathbf{r}_1)\psi^{(n)}(\mathbf{r}_2), \tag{B10}$$

$$\widetilde{U}_{\rm ext}(\mathbf{r};t)=\sum_m U^{(m)}_{\rm ext}(t)\psi^{(m)}(\mathbf{r}).$$

In this basis, the static structure function has the form (2.17), and the direct correlation function is

$$\widetilde{X}(\mathbf{r}_1,\mathbf{r}_2)=\delta(\mathbf{r}_1-\mathbf{r}_2)-\sum_m \psi^{(m)}(\mathbf{r}_1)\psi^{(m)}(\mathbf{r}_2). \tag{B11}$$

Projecting the equations of motion (A22) and (A18) on the Feynman states $|\psi^{(m)}\rangle$ produces the one-body equation

$$i\hbar\frac{\partial r_m}{\partial t}=\hbar\omega_m r_m+\frac{1}{2}\sum_{st} V^{(m)}_{st}\delta X_{st}+2U^{(m)}_{\rm ext}(t) \tag{B12}$$

and the two-body equation

$$\left[i\hbar\frac{\partial}{\partial t}-\hbar\omega_m-\hbar\omega_n\right]\delta X_{nm}=i\hbar\int d^3r\widetilde{\mathbf{j}}(\mathbf{r})\cdot\widetilde{\mathbf{W}}_{mn}(\mathbf{r}), \tag{B13}$$

where

$$\widetilde{\mathbf{W}}_{mn}(\mathbf{r})=\phi^{(m)}(\mathbf{r})\nabla\zeta^{(n)}(\mathbf{r})+\phi^{(n)}(\mathbf{r})\nabla\zeta^{(m)}(\mathbf{r})+\sqrt{\rho_1(\mathbf{r})}\nabla X_{mn}(\mathbf{r}) \tag{B14}$$

with

$$X_{mn}(\mathbf{r})=\frac{1}{\sqrt{\rho_1(\mathbf{r})}}\int d^3r_1d^3r_2\phi^{(m)}(\mathbf{r}_1)\phi^{(n)}(\mathbf{r}_2)\widetilde{X}_3(\mathbf{r}_1,\mathbf{r}_2,\mathbf{r}) \tag{B15}$$

and

$$V^{(s)}_{mn}=\frac{\hbar^2}{2m}\int d^3r\frac{\psi^{(s)}(\mathbf{r})}{\sqrt{\rho_1(\mathbf{r})}}\nabla\cdot[\sqrt{\rho_1(\mathbf{r})}\widetilde{\mathbf{W}}_{st}(\mathbf{r})]. \tag{B16}$$

To eliminate the current from Eq. (B13) we write

$$\widetilde{\mathbf{j}}(\mathbf{r}_1)=\frac{i\hbar}{2m}\left[\sqrt{\rho_1(\mathbf{r}_1)}\nabla_1\frac{1}{\sqrt{\rho_1(\mathbf{r}_1)}}\delta\widetilde{v}_1(\mathbf{r}_1)-\frac{1}{2}\sum_{mn}\widetilde{\mathbf{W}}_{mn}(\mathbf{r}_1)\delta\widetilde{X}_{mn}\right]. \tag{B17}$$

We can now combine Eqs. (A15), (B13), and (B17) and obtain

$$\left[i\hbar\frac{\partial}{\partial t}-\hbar\omega_m-\hbar\omega_n\right]\delta X_{nm}-\frac{\hbar^2}{4m}\sum_{st}\int d^3r\mathbf{W}_{mn}(\mathbf{r})\cdot\mathbf{W}_{st}(\mathbf{r})\delta X_{st}=\sum_s V^{(s)}_{mn}r_s. \tag{B18}$$

To get the expression for the response function, we now make a harmonic expansion of the external field and the fluctuations

$$U^{(m)}_{\rm ext}(t)=U^{(m)}[e^{-i\omega t}+e^{i\omega t}],$$

$$r_m(t)=x_me^{-i\omega t}+y_me^{i\omega t},$$

$$\delta X_{mn}(t)=x_{mn}e^{-i\omega t}+y_{mn}e^{i\omega t}, \tag{B19}$$

where we can assume that the x_m, y_m and x_{mn}, y_{mn} are real. Defining

$$T_{mn,st}(\omega)=\hbar[\omega_n+\omega_m-\omega]\delta_{ms}\delta_{nt}+\frac{\hbar^2}{4m}\int d^3\mathbf{r}\widetilde{\mathbf{W}}_{mn}(\mathbf{r})\cdot\widetilde{\mathbf{W}}_{st}(\mathbf{r}) \tag{B20}$$

and separating the portions with positive and negative frequency allows us to formally solve for the one- and two-body equations for the x_m, y_m and the x_{mn} and y_{mn}:

$$x_{mn}=-\sum_{r,pq}[T^{-1}(\omega)]_{mn,pq}\widetilde{V}^{(r)}_{pq}x_r,$$

$$y_{mn}=-\sum_{r,pq}[T^{-1}(-\omega)]_{mn,pq}\widetilde{V}^{(r)}_{pq}y_r,$$

$$\hbar(\omega-\omega_s)x_s=\frac{1}{2}\sum_{mn}\widetilde{V}^{(s)}_{mn}x_{mn}+2U^{(s)}_{\rm ext}, \tag{B21}$$

$$\hbar(-\omega-\omega_s)y_s=\frac{1}{2}\sum_{mn}\widetilde{V}^{(s)}_{mn}y_{mn}+2U^{(s)}_{\rm ext},$$

and obtain the full solutions of the problem:

$$\sum_t E_{st}(\omega)x_t=2U^{(s)}_{\rm ext},$$

$$\sum_t E_{st}(-\omega)y_t=2U^{(s)}_{\rm ext},$$

with

$$E_{st}(\omega)=\hbar(\omega-\omega_s)\delta_{st}+\frac{1}{2}\sum_{mn,pq}\widetilde{V}^{(s)}_{mn}[T^{-1}(\omega)]_{mn,pq}\widetilde{V}^{(t)}_{pq}. \tag{B22}$$

Evidently, we can identify $E_{st}(\omega)$ with the inverse of the one-phonon Green's function

$$G_{st}(\omega)=[\hbar(\omega-\omega_s+i\epsilon)\delta_{st}+\Sigma_{st}(\omega)]^{-1} \tag{B23}$$

with the self-energy

$$\Sigma_{st}(\omega)=\frac{1}{2}\sum_{mn,pq}\widetilde{V}^{(s)}_{mn}[T^{-1}(\omega)]_{mn,pq}\widetilde{V}^{(t)}_{pq}. \tag{B24}$$

We are now ready to calculate the real part of the density fluctuations:

$$\begin{aligned}\mathrm{Re}r_s(t)&=\frac{1}{2}[x_s+y_s][e^{-i\omega t}+e^{i\omega t}]\\&=\sum_t[G_{st}(\omega)+G_{st}(-\omega)]\widetilde{U}^{(t)}_{\rm ext}[e^{-i\omega t}+e^{i\omega t}].\end{aligned} \tag{B25}$$

The term in the square bracket can be identified with the density-density response function $\chi_{st}(\omega)$ in Feynman space. The coordinate representation is then

$$\chi(\mathbf{r}_1,\mathbf{r}_2;\omega)=\sum_{st}\sqrt{\rho_1(\mathbf{r}_1)}\phi^{(s)}(\mathbf{r}_1)[G_{st}(\omega)+G_{st}(-\omega)]\phi^{(t)}(\mathbf{r}_2)\sqrt{\rho_1(\mathbf{r}_2)}. \tag{B26}$$

The *normal modes* of the system are given, as usual, by the singularities of the response function, in other words by the solutions of the generalized eigenvalue problem

$$\sum_t E_{st}(\omega)x_t=0. \tag{B27}$$

In the nonuniform geometry, it is presently computationally too time consuming to keep the off-diagonal term of the propagator (B20). If we keep only the diagonal terms of $[T^{-1}(\omega)]_{mn,st}$, we recover the CBF-BW perturbation theory derived by Chang and Campbell[12] for the uniform system.

$$\Sigma^{\rm CBF}_{st}(\omega)=\frac{1}{2}\sum_{mn}\frac{\widetilde{V}^{(s)}_{mn}\widetilde{V}^{(t)}_{mn}}{\hbar(\omega_m+\omega_n-\omega)}, \tag{B28}$$

cf. Eqs. (B20) and (B24). We will use the same approximation for the numerical parts of this paper.

To complete this appendix, we display the ''three-phonon'' vertex function $V^{(t)}_{mn}$:

$$\begin{aligned}\widetilde{V}^{(t)}_{mn}&=\int d^3\mathbf{r}_1\phi^{(t)}(\mathbf{r}_1)\widetilde{V}_{mn}(\mathbf{r}_1)=-\frac{\hbar^2}{2m}\int d^3\mathbf{r}_1\nabla_1\left[\frac{\psi^{(t)}(\mathbf{r}_1)}{\sqrt{\rho_1(\mathbf{r}_1)}}\right]\cdot\{\xi^{(m)}(\mathbf{r}_1)\nabla_1\xi^{(n)}(\mathbf{r}_1)+\xi^{(n)}(\mathbf{r}_1)\nabla_1\xi^{(m)}(\mathbf{r}_1)\}\\&-\int d^3\mathbf{r}_1\widetilde{X}_{mn}(\mathbf{r}_1)H_1\psi^{(t)}(\mathbf{r}_1)=[\widetilde{V}^{(t)}_{mn}]_0+\omega_t\widetilde{X}_{mnt}=[\widetilde{V}^{(t)}_{mn}]_0+\frac{\omega_t\widetilde{V}_{mnt}}{\omega_m+\omega_n+\omega_t},\end{aligned} \tag{B29}$$

where

$$[\widetilde{V}^{(t)}_{mn}]_0=\frac{\hbar^2}{2m}\int d^3\mathbf{r}_1\left[\frac{\psi^{(t)}(\mathbf{r}_1)}{\sqrt{\rho_1(\mathbf{r}_1)}}\right]\nabla_1\cdot\{\xi^{(m)}(\mathbf{r}_1)\nabla_1\xi^{(n)}(\mathbf{r}_1)+\xi^{(n)}(\mathbf{r}_1)\nabla_1\xi^{(m)}(\mathbf{r}_1)\}, \tag{B30}$$

$$\tilde{V}_{mnt} = -\frac{\hbar^2}{2m}\int d^3\mathbf{r}_1\{\xi^{(m)}(\mathbf{r}_1)\nabla_1\zeta^{(n)}(\mathbf{r}_1)\cdot\nabla_1\zeta^{(t)}(\mathbf{r}_1)+\text{cycl.}\}, \tag{B31}$$

note that V_{mnt} is the three-body vertex of the ground-state theory. Inclusion of this term is necessary to obtain the correct density dependence of the roton energy in the bulk liquid.[12]

APPENDIX C: SUM RULES

In this appendix we will prove that first two moments of the improved dynamic structure function are identical to those of the Feynman approximation, in particular that the static structure function obtained within our theory — i.e., including time-dependent pair fluctuations — is *identical* to the one of the ground-state theory. In Eq. (2.18), we have expressed the density-density response function in coordinate space as

$$\chi^{\mathrm{CBF}}(\mathbf{r},\mathbf{r}',\omega) = \sqrt{\rho_1(\mathbf{r})}\sum_{st}\ \phi^{(s)}(\mathbf{r})\chi^{\mathrm{CBF}}_{st}(\omega)\phi^{(t)}(\mathbf{r}')\sqrt{\rho_1(\mathbf{r}')} \tag{C1}$$

with the matrix representation of the density-density response function

$$\chi^{\mathrm{CBF}}_{st}(\omega) = [G^{\mathrm{CBF}}_{st}(\omega) + G^{\mathrm{CBF}}_{st}(-\omega)], \tag{C2}$$

where (cf. Eq. (B23)] $G^{\mathrm{CBF}}_{st}(\omega)$ is the three-phonon approximation of the Green's function

$$G^{\mathrm{CBF}}_{st}(\omega) = [\hbar(\omega-\omega_t+i\epsilon)\delta_{st}+\Sigma^{\mathrm{CBF}}_{st}(\omega)]^{-1} \tag{C3}$$

with the self-energy correction (B28).

In the Feynman basis, ω^0 and the ω^1 sum rules simply state that

$$-\mathrm{Im}\int_0^\infty \frac{d(\hbar\omega)}{\pi}\chi_{st}(\omega) = \delta_{st} \tag{C4}$$

and

$$-\mathrm{Im}\int_0^\infty \frac{d(\hbar\omega)}{\pi}\hbar\omega\chi_{st}(\omega) = \hbar\omega_s\delta_{st}. \tag{C5}$$

We will follow the general procedure outlined in Ref. 17. First, we have to show that $G^{\mathrm{CBF}}_{st}(\omega)$ is, as a function of ω, analytic everywhere off the real axis. We will prove this by first assuming the converse and showing it leads to a contradiction. Let us assume that $G^{\mathrm{CBF}}_{st}(\omega)$ is singular for some complex ω. This assumption is equivalent to assuming that there is a *complex* value of ω for which the nonlinear eigenvalue equation (2.22) has a solution, i.e., explicitly that

$$\hbar\omega\varphi_s = \sum_t\left[\hbar\omega_t\delta_{st} - \sum_{mn}\frac{V^{(s)}_{mn}V^{(t)}_{mn}}{\hbar(\omega_m+\omega_n-\omega)}\right]\varphi_t. \tag{C6}$$

Without loss of generality, we can assume that φ_s is normalized. Projecting Eq. (3.6) on φ_s gives

$$\hbar\omega = \hbar\omega_s - \frac{1}{2}\sum_{mn,st}\frac{\varphi_s V^{(s)}_{mn}V^{(t)}_{mn}\varphi_t}{\hbar(\omega_m+\omega_n-\omega)}. \tag{C7}$$

Let us assume that ω is complex and can be written as

$$\omega = \omega_R + i\omega_I. \tag{C8}$$

The imaginary part of Eq. (C7) is then equivalent to

$$1 = -\frac{1}{2}\sum_{mn,ij}\frac{\varphi_s V^{(s)}_{mn}V^{(t)}_{mn}\varphi_t}{[\hbar(\omega_m+\omega_n-\omega_R)]^2+(\hbar\omega_I)^2}. \tag{C9}$$

This equation obviously cannot be fulfilled and, hence, the nonliner eigenvalue problem (C6) has only real solutions. Therefore $G^{\mathrm{CBF}}_{st}(\omega)$ is analytic everywhere off the real axis. Two more important properties, which can be read directly off Eqs. (C3) and (B28) are that $G^{\mathrm{CBF}}_{st}(\omega)$ is real on the negative real ω axis, and that

$$G^{\mathrm{CBF}}_{st}(\omega) = \frac{\delta_{st}}{\hbar(\omega-\omega_s+i\epsilon)} + O(\omega^{-3}) \quad (\text{as}|\omega|\to\infty). \tag{C10}$$

We are now ready to verify the ω^0 and the ω^1 sum rules. For the ω^0 sum rule (C4), the frequency integration is easily carried out by the usual contour integration procedure:

$$\int_0^\infty\frac{d(\hbar\omega)}{\pi}\mathrm{Im}[G^{\mathrm{CBF}}_{st}(\omega)+G^{\mathrm{CBF}}_{st}(-\omega)] = \int_{-\infty}^{\infty}\frac{d(\hbar\omega)}{\pi}\mathrm{Im}[G^{\mathrm{CBF}}_{st}(\omega)]. \tag{C11}$$

Since $G^{\mathrm{CBF}}_{st}(\omega)$ has no poles in the upper half plane, we can deform the contour to a large semicircle in the upper half plane. Hence, due to (C10) we obtain for the integral (C11)

$$\mathrm{Im}\int_{-\infty}^{\infty}\frac{d(\hbar\omega)}{\pi}G^{\mathrm{CBF}}_{st}(\omega) = \delta_{st} \tag{C12}$$

which is the identity we sought to prove.

The proof of the first-order sum rule (C5) is analogous. Let us calculate the integral

$$-\int_0^\infty \frac{d(\hbar\omega)}{\pi}[\hbar\omega-\hbar\omega_s]\mathrm{Im}\chi_{st}(\omega)=\int_0^\infty \frac{d(\hbar\omega)}{\pi}[\hbar\omega-\hbar\omega_s]\mathrm{Im}G_{st}^{\mathrm{CBF}}(\omega)=\mathrm{Im}\int_{-\infty}^{\infty}\frac{d(\hbar\omega)}{\pi}[\hbar\omega-\hbar\omega_s]G_{st}^{\mathrm{CBF}}(\omega). \tag{C13}$$

In both of the above steps we have used that $\mathrm{Im}G_{st}^{\mathrm{CBF}}(\omega)=0$ on the negative real axis. The last integral can again be evaluated by contour integration. Due to the asymptotic behavior (C10) we can close the contour integral in the upper half plane. Letting $\hbar\omega=\hbar\omega_s+Re^{i\phi}$,

$$\mathrm{Im}\int_{-\infty}^{\infty}\frac{d(\hbar\omega)}{\pi}G_{st}^{\mathrm{CBF}}(\omega)[\hbar\omega-\hbar\omega_s]=-\mathrm{Im}\,i\lim_{R\to\infty}\int_0^\pi\frac{d\phi}{\pi}Re^{i\phi}G_{st}^{\mathrm{CBF}}(\omega)[\hbar\omega-\hbar\omega_s]=-\lim_{R\to\infty}\mathrm{Im}\left[\frac{2R}{\pi}+O(R^{-1})\right]=0. \tag{C14}$$

This is the relation we wanted to prove.

APPENDIX D: PARTICLE CURRENTS

Since the $\delta\tilde{v}(\mathbf{r})$ are obtained in the Feynman basis, it is also convenient to represent the particle currents by the same basis states. Operating on Eq. (B17) from the left with the Feynman states we get

$$\begin{aligned}\tilde{\mathbf{j}}^t(\omega)&=\langle\phi^{(t)}(\mathbf{r}_1)|\tilde{\mathbf{j}}(\mathbf{r}_1)\rangle\\&=\frac{i\hbar}{2m}\left[\left\langle\phi^{(t)}(\mathbf{r}_1)\right|\sqrt{\rho_1(\mathbf{r}_1)}\nabla_1\frac{1}{\sqrt{\rho_1(\mathbf{r}_1)}}\delta\tilde{v}_1(\mathbf{r}_1)\right\rangle\\&\quad-\frac{1}{2}\sum_{mn}\langle\phi^{(t)}(\mathbf{r}_1)|\tilde{\mathbf{W}}_{mn}(\mathbf{r}_1)\rangle\delta\tilde{X}_{mn}\Bigg]\end{aligned} \tag{D1}$$

which can be rewritten as

$$\tilde{\mathbf{j}}^t(\omega)=\frac{i\hbar}{2m}\sum_s\left[\mathbf{D}_{ts}v_s-\frac{1}{2}\sum_{mn}\frac{\tilde{\mathbf{W}}_{mn}^t\tilde{V}_{mn}^s v_s}{\hbar(\omega_m+\omega_n-\omega)}\right], \tag{D2}$$

where

$$\mathbf{D}_{ts}=\left\langle\phi^{(t)}(\mathbf{r})\right|\sqrt{\rho_1(\mathbf{r}_1)}\nabla_1\frac{1}{\sqrt{\rho_1(\mathbf{r}_1)}}\left|\psi^{(s)}(\mathbf{r})\right\rangle,$$

$$\tilde{\mathbf{W}}_{mn}^t=[\tilde{\mathbf{W}}_{mn}^t]_0+\sum_p\mathbf{D}_{tp}\tilde{X}_{mnp}, \tag{D3}$$

$$[\tilde{\mathbf{W}}_{mn}^t]_0=\left\langle\phi^{(t)}(\mathbf{r})\right|\frac{1}{\sqrt{\rho_1(\mathbf{r}_1)}}[\zeta^n(\mathbf{r})\nabla\xi^m(\mathbf{r})+\zeta^m(\mathbf{r})\nabla\xi^n(\mathbf{r})]\Bigg\rangle. \tag{D4}$$

A useful property of Eq. (D2) is obtained by operating on Eq. (D2) with $\mathbf{D}_{st}^{-1}$. With some manipulation we can show for the *collective modes*, i.e., for the solutions of the nonlinear eigenvalue equation (2.22) that

$$v_s=\frac{2m}{i\hbar\omega}\sum_t\mathbf{D}_{st}^{-1}\cdot\tilde{\mathbf{j}}^t(\omega), \tag{D5}$$

where we have defined

$$\mathbf{D}_{st}^{-1}=\frac{\hbar^2}{2m}\left\langle\psi^{(t)}(\mathbf{r})\right|\sqrt{\rho_1(\mathbf{r}_1)}\nabla_1\frac{1}{\sqrt{\rho_1(\mathbf{r}_1)}}\left|\phi^{(s)}(\mathbf{r})\right\rangle,$$

$$\sum_t\mathbf{D}_{st}^{-1}\cdot\mathbf{D}_{tp}=\hbar\omega_s\delta_{sp},$$

$$\sum_t\mathbf{D}_{st}^{-1}\cdot\mathbf{W}_{mn}^t=[\tilde{V}_{mn}^{(s)}]_0. \tag{D6}$$

Within our numerical calculations, we found that the identity (D6) provides a useful test of the numerical accuracy of our calculation. Specifically, we have calculated Eq. (D5) in our truncated basis in order to determine how many intermediate states we needed to keep such that we obey this identity is satisfied within an accuracy of about 1%.

*Present address Los Alamos National Laboratory, Gp. T1, MS B221, Los Alamos, NM 87545.

†Present address: Department of Physics, Clark Atlanta University, J. P. Brawley Drive, Atlanta, GA 30314.

[1] B. E. Clements, J. L. Epstein, E. Krotscheck, and M. Saarela, Phys. Rev. B **48**, 7450 (1993).

[2] B. E. Clements *et al.*, Phys. Rev. B **50**, 6958 (1994).

[3] B. E. Clements *et al.*, preceding paper, Phys. Rev. B **53**, 12 242 (1996).

[4] B. E. Clements, H. Forbert, E. Krotscheck, and M. Saarela, J. Low Temp. Phys. **95**, 849 (1994).

[5] M. Saarela, Phys. Rev. B **33**, 4596 (1986).

[6] M. Saarela and J. Suominen, in *Condensed Matter Theories*, edited by J. S. Arponen, R. F. Bishop, and M. Manninen (Plenum, New York, 1988), Vol. 3, p. 157.

[7] J. Suominen and M. Saarela, in *Condensed Matter Theories*, edited by J. Keller (Plenum, New York, 1989), Vol. 4, p. 377.

[8] P. Kramer and M. Saraceno, *Geometry of the Time-Dependent Variational Principle in Quantum Mechanics*, Lecture Notes in Physics Vol. 140 (Springer, Berlin, 1981).

[9] A. K. Kerman and S. E. Koonin, Ann. Phys. (NY) **100**, 332 (1976).

[10] R. A. Aziz *et al.*, J. Chem. Phys. **70**, 4330 (1979).

[11] R. P. Feynman and M. Cohen, Phys. Rev. **102**, 1189 (1956).

[12] C. C. Chang and C. E. Campbell, Phys. Rev. B **13**, 3779 (1976).
[13] H. W. Jackson and E. Feenberg, Rev. Mod. Phys. **34**, 686 (1962).
[14] H. W. Jackson, Phys. Rev. A **8**, 1529 (1973).
[15] R. P. Feynman, Phys. Rev. **94**, 262 (1954).
[16] E. Krotscheck, Phys. Rev. B **31**, 4258 (1985).
[17] H. W. Jackson, Phys. Rev. A **9**, 964 (1974).
[18] A. Lastri, F. Dalfovo, J. Pitaevskii, and S. Stringari, J. Low Temp. Phys. **98**, 227 (1995).
[19] S. A. Chin and E. Krotscheck, Phys. Rev. B **52**, 10 405 (1996).
[20] E. Krotscheck, Phys. Rev. B **33**, 3158 (1986).
[21] R. A. Cowley and A. D. B. Woods, Can. J. Phys. **49**, 177 (1971).
[22] C. E. Campbell, in *Progress in Liquid Physics*, edited by C. A. Croxton (Wiley, London, 1977), Chap. 6, pp. 213–308.
[23] W. Montfrooij and I. de Schepper, Phys. Rev. B **51**, 15 607 (1995).
[24] S. Moroni, D. Ceperley, and G. Senatore (unpublished).
[25] L. Reatto, S. A. Vitiello, and G. L. Masserini, J. Low Temp. Phys. **93**, 879 (1993).
[26] D. Pines and P. Nozieres, *The Theory of Quantum Liquids* (Addison Wesley Publishing Co., New York, 1990), Vol. II.
[27] A. D. Jackson, B. K. Jennings, A. Lande, and R. A. Smith, Phys. Rev. B **24**, 105 (1981).
[28] M. Saarela, B. E. Clements, E. Krotscheck, and F. V. Kusmartsev, J. Low Temp. Phys. **93**, 971 (1993).
[29] H. J. Lauter, H. Godfrin, and H. Wiechert, in *Proceedings of the Second International Conference on Phonon Physics*, edited by J. Kollàr, N. Kroo, M. Meynhard, and T. Siklos (World Scientific, Singapore, 1985), p. 842.
[30] H. J. Lauter, H. Godfrin, V. L. P. Frank, and P. Leiderer, in *Excitations in Two-Dimensional and Three-Dimensional Quantum Fluids*, Vol. 257 of *NATO Advanced Study Institute, Series B: Physics*, edited by A. F. G. Wyatt and H. J. Lauter (Plenum, New York, 1991), p. 419.
[31] B. E. Clements, E. Krotscheck, J. A. Smith, and C. E. Campbell, Phys. Rev. B **47**, 5239 (1993).
[32] E. Feenberg, *Theory of Quantum Liquids* (Academic, New York, 1969).
[33] W. G. Stirling, in *Proceedings of the Second International Conference on Phonon Physics*, edited by J. Kollàr, N. Kroo, M. Meynhard, and T. Siklos (World Scientific, Singapore, 1985), p. 829.
[34] O. W. Dietrich, E. H. Graf, C. H. Huang, and L. Passell, Phys. Rev. A **5**, 1377 (1972).
[35] W. G. Stirling, in *Interpretation of Inelastic Light Scattering Measurements in ^{4}He*, Vol. 257 of *NATO Advanced Study Institute, Series B: Physics*, edited by A. F. G. Wyatt and H. J. Lauter (Plenum, New York, 1991), p. 47.